iScience

CellPress
OPEN ACCESS

Article

A robust platform for high-throughput screening of therapeutic strategies for acute and chronic spinal cord injury

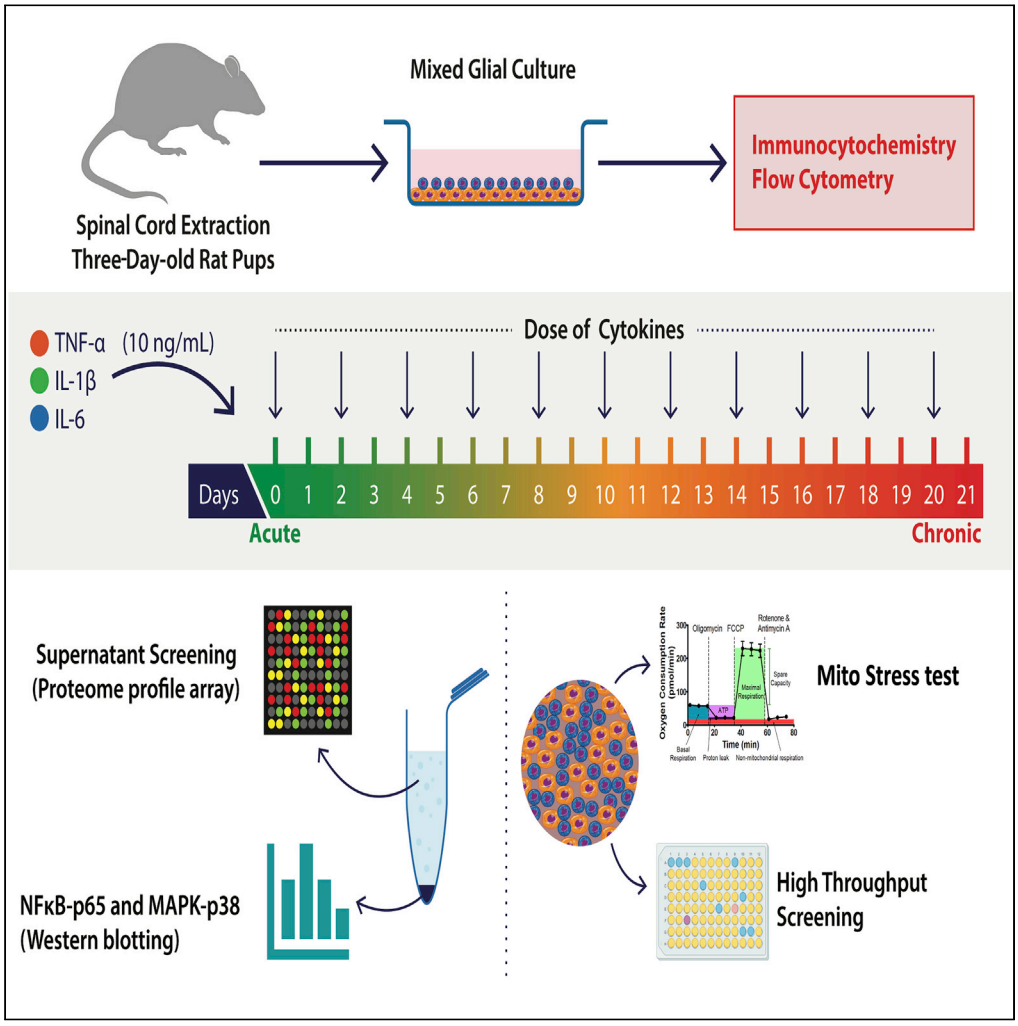

Vaibhav Patil, Enda O'Connell, Leo R. Quinlan, Howard Fearnhead, Siobhan McMahon, Abhay Pandit

abhay.pandit@nuigalway.ie

HIGHLIGHTS

An *in vitro* MGC model replicates the inflammatory phases associated with SCI

Differential modulation in NF-κB, MAPK, and immunomodulatory pathways over 21 days

Change in mitochondrial bioenergetics over seven days

ELISA-based HTS platform using CINC-3 as a biomarker is established

Patil et al., iScience *24*, 102182
March 19, 2021
https://doi.org/10.1016/j.isci.2021.102182

iScience

CellPress
OPEN ACCESS

Article

A robust platform for high-throughput screening of therapeutic strategies for acute and chronic spinal cord injury

Vaibhav Patil,[1] Enda O'Connell,[3] Leo R. Quinlan,[1,4] Howard Fearnhead,[5] Siobhan McMahon,[1,2] and Abhay Pandit[1,6,*]

SUMMARY

Astrocytes and microglia are critical regulators of inflammatory cascade after spinal cord injury (SCI). Existing glial *in vitro* studies do not replicate inflammatory phases associated with SCI. Here, we report an *in vitro* model of mixed glial culture where inflammation is induced by the administration of pro-inflammatory cytokines (tumor necrosis factor-α, interleukin-1β, and interleukin-6) to promote pathologically relevant "acute" and "chronic" inflammatory phases. We observed SCI relevant differential modulation of inflammatory pathways, cytokines, chemokines, and growth factors over 21 days. Mitochondrial dysfunction was associated with a cytokine combination treatment. Highly expressed cytokine induced neutrophil chemoattractant (CINC-3) chemokine was used as a biomarker to establish an enzyme-linked immunosorbent assay-based high-throughput screening (HTS) platform. We screened a 786-compound drug library to demonstrate the efficacy of the HTS platform. The developed model is robust and will facilitate *in vitro* screening of anti-reactive glial therapeutics for the treatment of SCI.

INTRODUCTION

Spinal cord injury (SCI) is a catastrophic event that results in severe primary mechanical trauma followed by more complex secondary injury (Kabu et al., 2015). In the secondary injury process, inflammation is one of the critical hallmarks due to activation of highly motile microglia, astrocytes, and infiltration of blood-borne immune cells at the site of injury (DiSabato et al., 2016). The dual activation (microglia and astrocytes) sparks a burst release of pro-inflammatory cytokines such as tumor necrosis factor-α (TNF-α), interleukin (IL)-1β, and interleukin (IL)-6 at the injury site (Donnelly and Popovich, 2008). These cytokines activate various pathways such as nuclear factor kappa-light-chain-enhancer of activated B cells (NF-κB), mitogen-activated protein kinase (MAPK), nitric oxide (NO) synthase, and chemokine signaling by activating their corresponding receptors which plays a vital role in upregulating the inflammatory cascade (Becher et al., 2017). This leads to the secretion of inflammatory biomarkers such as high mobility group box 1 (HMGB1), NO (Pineau and Lacroix, 2007), and cytokine-induced neutrophil chemoattractant (CINC-3) also known as macrophage inflammatory protein (MIP)-2 (Chio et al., 2019). Glial activation also induces reactive oxygen species (ROS) production, which further elevates the inflammation and upregulates the corresponding biomarkers (Xu et al., 2005). These inflammatory stimuli can persist from acute to chronic phases after the initial trauma (Norenberg et al., 2004). Studying these biomarkers helps us to understand the activation of inflammation and the development of therapeutics in SCI.

Most of the glial *in vitro* studies related to inflammation are focused on studying molecular mechanisms involved in the acute phase and are unspecific with no emphasis on the chronic phase (Alizadeh et al., 2019). Therefore, creating an *in vitro* model that mimics glia-specific chronic inflammatory conditions is paramount. During inflammation, it is known that astrocytes and microglia are involved in cross talk in terms of regulation of inflammation. However, the mechanism of their co-operation is yet to be fully understood (Liu et al., 2011). Also, how they co-ordinate signals with each other under the influence of different cytokines is yet to be fully understood.

Over the last two decades, our understanding of the role of astrocytes and microglia in SCI has led to various strategies to overcome inflammation-induced pathological conditions (Möller and Boddeke,

[1]CÚRAM, SFI Research Centre for Medical Devices, National University of Ireland, Galway, Ireland

[2]Anatomy, National University of Ireland, Galway, Ireland

[3]Genomics and Screening Core Facility, National University of Ireland, Galway, Ireland

[4]Physiology, National University of Ireland, Galway, Ireland

[5]Pharmacology and Therapeutics, National University of Ireland, Galway, Ireland

[6]Lead contact

*Correspondence: abhay.pandit@nuigalway.ie

https://doi.org/10.1016/j.isci.2021.102182

2016). However, there is a lack of robust *in vitro* models that can provide not only the assessment of the progression of glial cell-derived inflammation but also a method for screening therapeutic interventions which help treatment options for SCI. Although drug screening has been carried out with BV2 microglial cell line (Mutemberezi et al., 2018) and RAW264.7 (Zhang et al., 2019) and THP-1 macrophages (Park, 2017) (Jhang et al., 2015), primary cultures have the advantage of more closely resembling the disease state. Hence, we have introduced a primary mixed glial-based, quantitative high-throughput screening (HTS) platform, using a CINC-3 chemokine, as a marker of inflammation.

Here, we report the development of a cytokine-induced inflamed mixed glial culture (MGC) *in vitro* model to study the acute and chronic inflammatory phases of SCI at the preclinical stage. Studies have demonstrated that astrocytes and microglia respond to the primary mechanical injury and become inflamed as early as day one after SCI (Sun et al., 2019); (Wang et al., 2019); therefore, we have considered one-day postinflammation as "acute" and 21-day postinflammation as "chronic". The pattern of the expression of NF-κB and MAPK pathways was studied over 21 days following inflammatory cytokine/s and lipopolysaccharide (LPS) treatment. Supernatant profiling was carried out to study the expression of chemokines, cytokines, and growth factors over 21 days. The bioenergetic phenotype of glia and mitochondrial respiration was studied over seven days after treatment. Finally, by using this model, we have demonstrated for the first time that our established model can be used to screen potent anti-inflammatory drugs. As a proof of concept, a CINC-3-based HTS was performed to demonstrate small volume, enzyme-linked immunosorbent assay (ELISA)-based compound primary screening, and further efficacy was assessed using secondary screening.

RESULTS

MGC containing microglia and astrocytes showed morphological changes upon cytokine combination treatment

The study aimed to prepare an *in vitro* model, which will represent the acute and chronic inflammatory state of SCI and use it as an HTS platform to identify anti-inflammatory compounds. The study was divided into various sections to understand immunomodulatory pathways at the translational level, mitochondrial response, and to demonstrate a high-throughput screen for compound screening (Figure 1). Microscopy details demonstrated that the spinal cord-derived MGC population mostly comprised astrocytes (glial fibrillary acidic protein, $GFAP^+$) and microglia $CD11b^+$ (Figure 2A). These results were further validated by using flow cytometry to confirm the presence of two of glial cell populations; quantification showed the presence of $GFAP^+$ astrocytes (33.33%) and $CD11b^+$ microglia (44.62%) (Figures 2D and 2E). No B-III $tubulin^+$ neurons (Figure 2C) were detected, in line with the absence of any neuronal growth factors or supplements (Gingras et al., 2007) in media. The remaining cells mostly comprised $olig2^+$ oligodendrocytes (Figure 2B).

Optimization of cytokine concentrations (TNF-α, IL-1β, and IL-6) involved treating cells with four concentrations of each cytokine (1, 10, 30, and 50 ng/mL) for 24 hr, and the expression of inducible nitric oxide synthase (iNOS) and nitrite release was assessed. All three cytokines (individually) not only changed the morphology of MGC from 10 ng/mL to 50 ng/mL doses (Figure S1A) but also increased nitrite production (Figures 2F–2H) due to the activation of iNOS (Figure 2I). Based on these data, a 10 ng/mL dose of each cytokine was found to be optimal and was used in all further experiments. Moreover, when MGC was treated with the cytokine combination (TNF-α+ IL-1β+ IL-6) with the dose of 10 ng/mL of each cytokine, there were morphological alterations in GFAP+ astrocytic processes (elongated and decreased roundness) (Figures 2J–2M). Microglia (CD11b+) also changed their shape to more circular (ameboid) (Figure S1B). The cytokine combination treatment also increased the nitrite production (Figure S1C). Further, the concentration of LPS sufficient to induce iNOS, nitrite production, and TNF-alpha production (Figures S1D–S2F) was determined to be 100 ng/mL. LPS was used as a control to compare with the cytokine group and was always added at the same time points on the same number of cells. We have observed that cultures were confluent and alive after 21 days without any treatment. Under cytokine combination treatment, we observed that cells were highly proliferative. In our LPS treatment group, we found that the cells were affected by treatment and that the viability of mixed glia decreased over time (Figure S1O).

Differential activation of NFκB-p65 and MAPK-p38 pathways over 21 days

It is essential to understand the effect of cytokine alone and in combination on MGC from the acute to the chronic stages of inflammation. Therefore, we selected multiple cytokine combinations and kept LPS as a

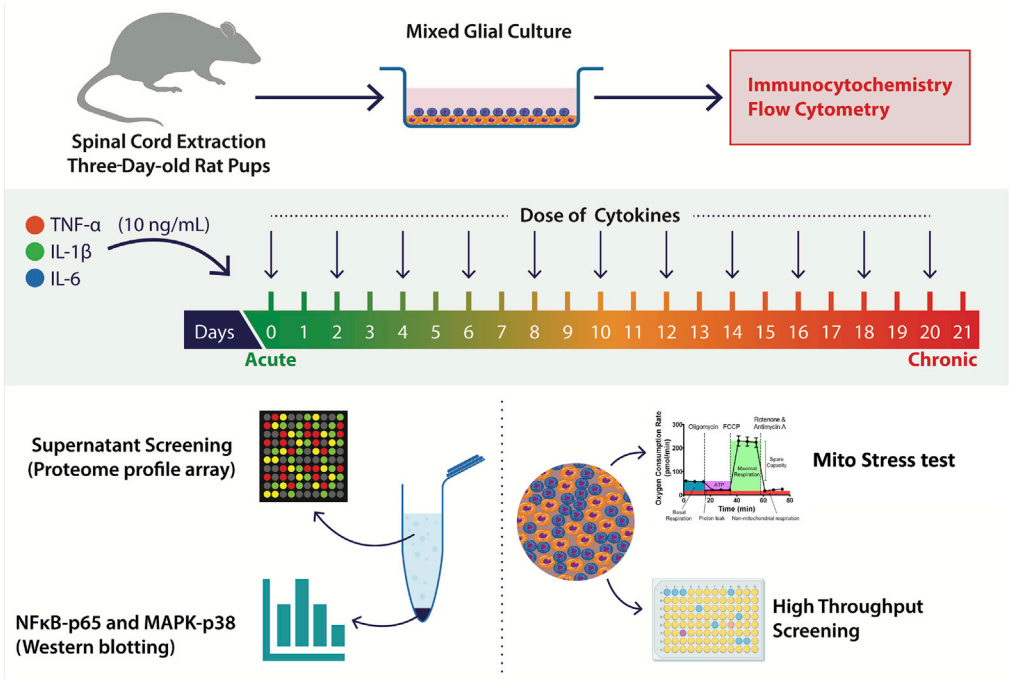

Figure 1. Workflow describing steps involved in the development of the MGC HTS model

MGCs were prepared from spinal cords isolated by the hydraulic extrusion technique from three-day-old postnatal rats. Immunocytochemistry and flow cytometry were performed to characterize the MGC, and further quantification of astrocytes, microglia, oligodendrocytes, and neurons was carried out. MGCs were treated with TNF-α, IL-1β, and IL-6 (10 ng/mL per cytokine) in combination/s for one day (acute) to 21 days (chronic). LPS (10 ng/mL) was used as a positive control. Treatments were given every alternate day (n = images from three experimental replicates). The supernatant was assayed using the Proteome Profiler Array (R&D Systems, Inc.). Total protein was extracted, and western blotting was performed to study the activation of NFκB-p65 and MAPK-p38 pathways (n = 3). Mitochondrial function was assessed by using Seahorse Mito Stress Test assay. MGCs were treated with TNF-α, IL-1β, and IL-6 (10 ng/mL per cytokine) for seven days (n = 3). Finally, an HTS platform was established that enabled identification of anti-inflammatory compounds.

positive control (Table S1). A dose of 10 ng/mL of each cytokine was given every alternate day to MGC, and on days 1, 4, 7, 10, 13, 16, 19, and 21, media were collected, and proteins were extracted from cells. The extracted protein samples were analyzed by western blotting to detect the expression of NFκB-p65 and p-38MAPK pathways (Figure 3A). This analysis was done to compare time points of each treatment. Analysis of the expression of phosphorylated p65 (for NFκB-p65 pathway) shows each cytokine combination had a variable effect not only on pathway activation but also on the level of activation (Figure 3J). Cytokine combinations with TNF-α alone or in combination with IL-1β and IL-6 and LPS treatment caused phosphorylation of p65 (P-p65) which increased from day one to day four and was downregulated at day seven; however, p65 phosphorylation was not statistically significant (Figures 3B, 3C, 3E, 3F, 3H, and 3I). Moreover, in these cytokine combinations, p65 phosphorylation increased on day 10 and then rapidly decreased from that point until day 21. Although the same trend was observed in the LPS treated group, it was not significant (Figure 3I). In all the groups where TNF-α was involved, strong activation was observed. In contrast, treatments with IL-1β or IL-6 alone did not activate the pathway significantly over 21 days when compared between days (Figures 3C and 3D).

As for phosphorylated p38 (for p38-MAPK pathway), we observed that each cytokine combination also had a variable effect not only on pathway activation but also on a level of activation (Figure 3S). However, unlike the NFκB-p65 pathway, with cytokine combinations and LPS treatments, phosphorylation of p38 did not increase from day one to day four and decreased at day seven (Figure 3S). Moreover, LPS showed a distinct pattern as it significantly activated the pathway at day one (Figure 3R). TNF-α treatment alone did not induce significant activation of the pathway from the acute to the chronic phase (Figure 3K). In IL-1β, IL-6, TNF-α+ IL-6, IL-1β+ IL-6, and TNF-α + IL-1β + IL-6 combinations, the pathway was significantly activated at day 13 and then rapidly decreased from there on till day 21 (Figures 3L, 3M, and 3O–3Q). However,

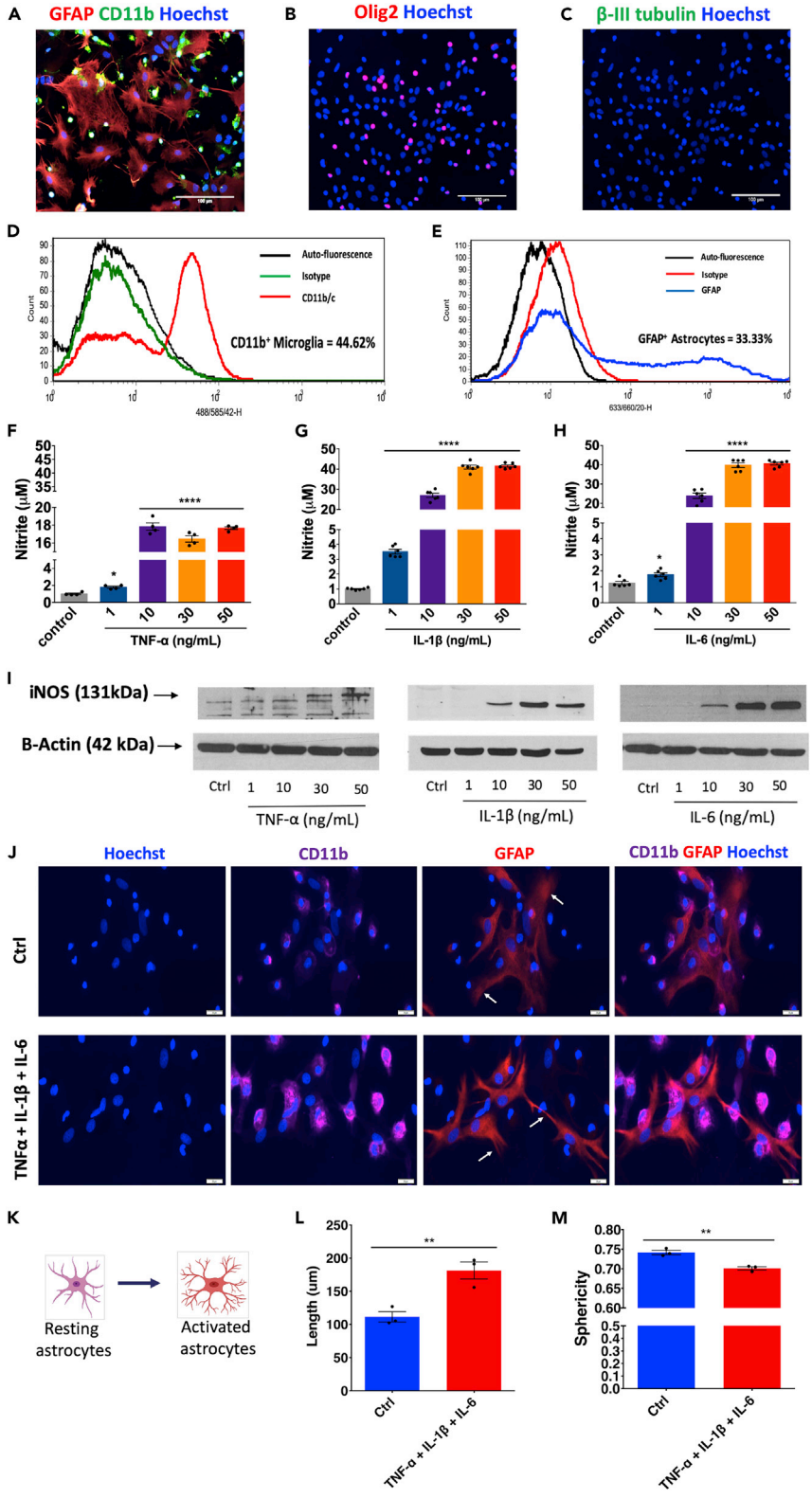
A
GFAP CD11b Hoechst
B
Olig2 Hoechst
C
β-III tubulin Hoechst
D
Auto-fluorescence
Isotype
CD11b/c
CD11b⁺ Microglia = 44.62%
Count
488/585/42-H
E
Auto-fluorescence
Isotype
GFAP
GFAP⁺ Astrocytes = 33.33%
Count
633/660/20-H
F
Nitrite (μM)
control
TNF-α (ng/mL)
G
Nitrite (μM)
control
IL-1β (ng/mL)
H
Nitrite (μM)
control
IL-6 (ng/mL)
I
iNOS (131kDa)
B-Actin (42 kDa)
Ctrl
TNF-α (ng/mL)
IL-1β (ng/mL)
IL-6 (ng/mL)
J
Hoechst
CD11b
GFAP
CD11b GFAP Hoechst
Ctrl
TNFα + IL-1β + IL-6
K
Resting astrocytes
Activated astrocytes
L
Length (um)
Ctrl
TNF-α + IL-1β + IL-6
M
Sphericity
Ctrl
TNF-α + IL-1β + IL-6

Figure 2. Characterization of MGC and optimization of pro-inflammatory cytokine dose and effect of the treatment on MGC phenotypes

(A–C) Immunostaining using GFAP, CD11b, and Olig2 markers showed the presence of astrocyte, microglia, and oligodendrocytes, respectively. The Beta III tubulin staining could not detect any neurons in MGC. n = 3, scale bar = 100 μm.

(D–E) Flow cytometry confirms the quantification of astrocytes and microglia in MGC.

(F–I) Griess assay and western blotting showing the production of nitrite and iNOS expression, respectively, under different dosage of TNF-α, IL-1β, and IL-6 treatment. A 10 ng/mL dose of each of cytokine was selected to be used for further studies. Data are expressed as mean ± standard error of the mean (SEM), n = two independent experiments each with two-three replicates; ****$p < 0.0001$, *$p < 0.05$ compared with the control group (24 hr), one-way analysis of variance (ANOVA), *post hoc* Tukey test.

(J) Effect of cytokine combination on astrocytes (GFAP, red) and microglia (CD11b, violet). Scale bar = 20 μm.

(K) Change in the morphology of astrocytes from resting to activated phase. Their processes become more ramified upon activation.

(L and M) Quantification of astrocytic processes shows processes that were (L) more elongated and (M) showed a decrease in roundness after cytokine combination treatment (24 hr). Data are represented as mean ± SEM, n = 3; **$p < 0.01$, Mann-Whitney U test (See also Figures S1 and S10).

TNF-α+ IL-1β combination treatment showed that the pathway was significantly activated at day one and 13 compared to that on other days (Figure 3N). Overall MAPK-p38 pathway was significantly activated at early time points, and the presence of IL-6 in the treatment group showed higher activation of this pathway at day 13. Therefore, the study of these pathways over a different time course with different cytokine combinations has allowed for a deeper understanding of the progression of the inflammation.

The supernatant (media) from cytokine combination-treated MGC showed differential upregulation of inflammatory molecules and biological functions upon proteome profiling.

The proteome profile array kit was used to assess the expression of chemokines, pro- and anti-inflammatory cytokines, and growth factors secreted by MGC (Figure 4A). Twelve blots showed the various expression patterns of proteins (79 analytes) from day one to day 21 under three conditions (control, cytokine combination, and LPS) (Figure S2). The heat map showed an increase in the production of the number of chemokines (CINC-3, monocyte chemoattractant protein-1, MIP-3α, and chemokine [C-C motif] ligands [CCL] 4), pro-inflammatory cytokines (IL-1ra, TNF-α, IL-1β, IL-6, and osteopontin), growth factors (insulin-like growth factor binding protein [IGFBP]-3, granulocyte colony-stimulating factor, Wnt1-inducible signaling pathway protein-1, and vascular endothelial growth factor [VEGF]), glycoproteins (galectin-3 and vascular cell adhesion molecule [VCAM]-1), matrix metalloproteins (MMP3 and MMP2), neutrophil gelatinase-associated lipocalin, cystatin-C, and cellular communication network factor-3 under the cytokine combination from day one to day 21 (Figures 4B and S4). We also observed a similar trend in the expression of growth factors that were not expressed upon the treatment, except IGFBP-2 and 3 which are involved in the p-53 apoptosis pathway (stress related) (Figure 4B). This is due to the change in fetal bovine serum (FBS) concentration from 10% to 1% in media. We observed upregulation of galectin-3, intercellular adhesion molecule (ICAM)-1, and VCAM-1 in cytokine combination-treated groups. Moreover, using Pearson's correlation hierarchical clustering metric, the treatment groups were separated to several clusters, illustrating the heterogenicity among control, cytokine combination, and LPS treatments. Also, it demonstrated the relationship between the time-dependent treatments (Figure 4B).

Proteome profile data were further analyzed using Ingenuity Pathway analysis (IPA) software to understand the modulation and involvement of upstream canonical pathways, mechanisms, and biological functions related to the regulation of neuroinflammation. We applied the cutoff of 1.5 for downstream and upstream canonical pathways. IPA analysis predicted that the HMBG1 pathway was highly expressed at day one and day 14 upon cytokine combination and day one, seven, and fourteen upon LPS treatment (Figures 4C and S3). This pathway has been well explored in SCI as it stimulates many inflammatory signals. Vitamin D receptor/retinoic X receptor pathway was activated at the later time points (days seven, 14, and 21) in cytokine combination- and LPS-treated groups. Liver X receptor/retinoic X receptor pathway was differentially regulated from day one to day 21, and the pattern of activation was different between the cytokine combination and the LPS groups (Figure 4C). IL-15- and IL-17-mediated pathways showed a similar response between cytokine combination- and LPS-treated groups (Figures 4C and S3). Except for day 14 of the cytokine combination group, the other time points showed unfavorable conditions for axonal guidance

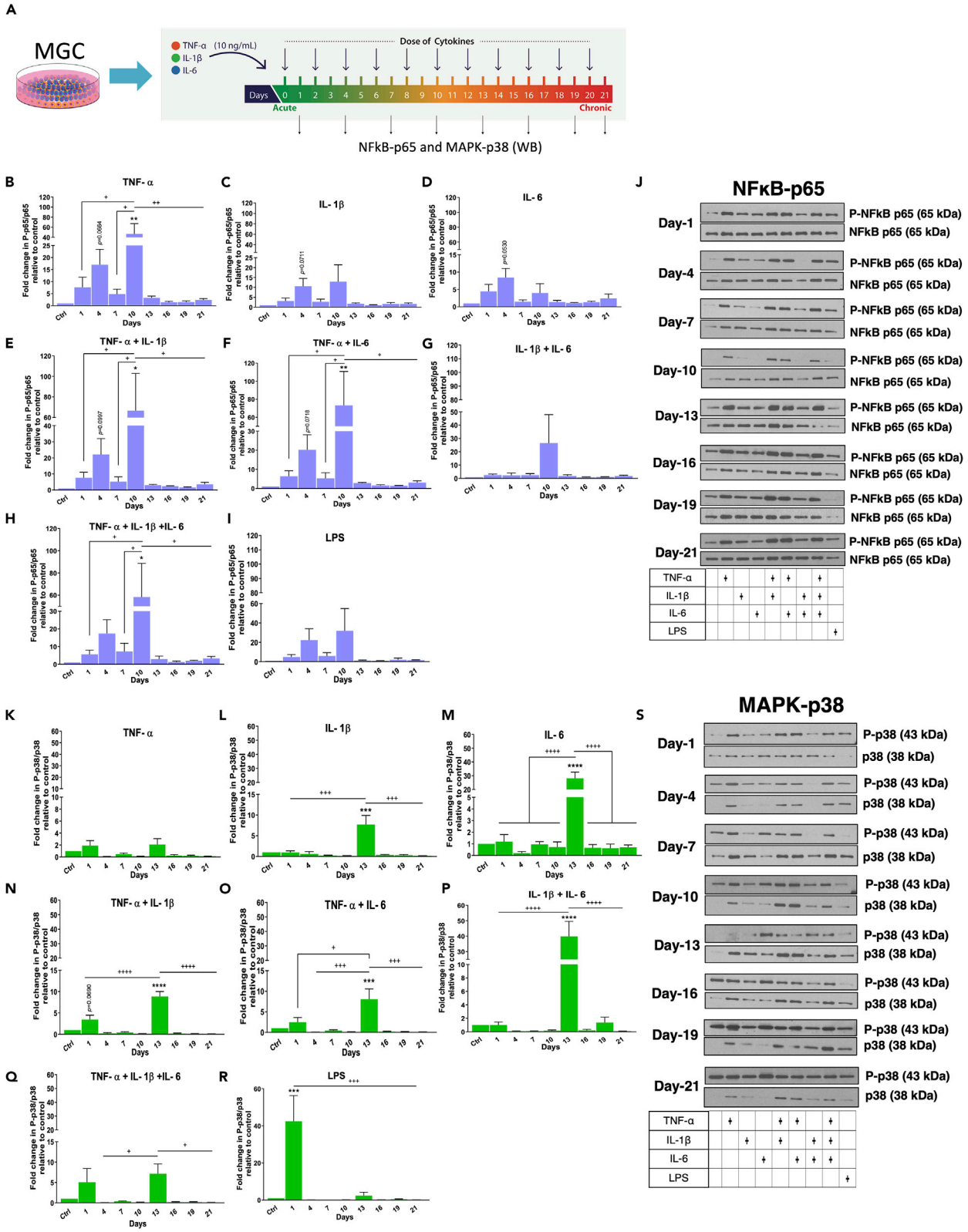
A
MGC
TNF-α (10 ng/mL)
IL-1β
IL-6
Dose of Cytokines
Days 0 1 2 3 4 5 6 7 8 9 10 11 12 13 14 15 16 17 18 19 20 21
Acute
Chronic
NFkB-p65 and MAPK-p38 (WB)
B TNF- α
C IL- 1β
D IL- 6
E TNF- α + IL- 1β
F TNF- α + IL-6
G IL- 1β + IL- 6
H TNF- α + IL- 1β +IL- 6
I LPS
Fold change in P-p65/p65 relative to control
Days
J NFκB-p65
Day-1
Day-4
Day-7
Day-10
Day-13
Day-16
Day-19
Day-21
P-NFkB p65 (65 kDa)
NFkB p65 (65 kDa)
TNF-α
IL-1β
IL-6
LPS
K TNF- α
L IL- 1β
M IL- 6
N TNF- α + IL- 1β
O TNF- α + IL- 6
P IL- 1β + IL- 6
Q TNF- α + IL- 1β +IL- 6
R LPS
Fold change in P-p38/p38 relative to control
S MAPK-p38
P-p38 (43 kDa)
p38 (38 kDa)

Figure 3. Cytokine combination treatments differentially activate NFκB-p65 and MAP-p38 pathways

Western blots show the quantification of the expression of P-NFκB-p65 and P-MAP-p38 from 24 hr up to 21 days upon various combinatorial treatments of TNF-α, IL-1β, and IL-6. The intensity of the P-NFκB-p65 was normalized to NFκB-p65, and the intensity of the P-p38-MAPAK was normalized to p38-MAPAK.

(A) Layout of the experiment.

(B–H) Upon the treatment of (B) TNF-α, (E) TNF-α and IL-1β, (F) TNF-α and IL-6, and (H) TNF-α, IL-1β, and IL-6 combinations, the pathway was highly activated from the acute to the subacute phase (day one to day ten). However, the combinations of (C) IL-1β, (D) IL-6, and (G) IL-1β and IL-6 treatments did not significantly regulate the pathway over the acute to the subacute phase.

(I) LPS did not induce the activation of the pathway significantly.

(J) Western blots.

All combinatorial treatments did not affect the pathway from day 13 to day 21.

(K–Q) (K) TNF-α treatment did not induce significant activation of the pathway from the acute to the chronic phase.

Upon treatment of (L) IL-1β, (M) IL-6, (O) TNF-α and IL-6, (P) IL-1β and IL-6, and (Q) TNF-α, IL-1β, and IL-6 combinations, the pathway was significantly activated at day 13. However, (N) TNF-α and IL-1β combination treatment showed the pathway was activated significantly at day one compared to other days except for day 13. In this combination also, the pathway was significantly activated at day 13.

(R) LPS induced the activation of the pathway at day one.

(S) Western blots.

Data are represented as mean ± SEM, n = three experimental replicates ****$p < 0.0001$, ***$p < 0.001$, **$p < 0.01$, *$p < 0.05$ compared with a control group (Ctrl). $^{++++}p < 0.0001$, $^{+++}p < 0.001$, $^{++}p < 0.01$, $^{+}p < 0.05$; one-way ANOVA, *post hoc* multiple comparison Tukey test (See also Table S1).

signaling. It also predicted that fibroblast growth factor and IL-22 were minimally expressed during all time points emphasizing the presence of inflammatory conditions (Figure 4C). This was further confirmed as we observed upstream regulators plotted as activation *Z* score showed higher expression of pro-inflammatory cytokines (HMGB1, IL-18, IL-17A, IL1, and IL1A) and lower expression of anti-inflammatory cytokines (IL-10, IL22, IL-13, and IL-5). Genes such as suppressor of cytokine signaling (SOCS)-3 and mothers against decapentaplegic homolog-3, which suppresses inflammatory stimulus, were downregulated (Figure S3). Also, phosphatase and tensin homolog (PTEN) reported to be involved in suppression of PI3/AKT/mTOR pathway, also downregulated. There were more ROS and hydrogen peroxide species (Figures S3 and 5); however, the superoxide dismutase-1 responsible for destroying free superoxide radicals was downregulated (Figure S3). This indicates the events causing mitochondrial damage and production of oxygen radicals after inflammation upon SCI. Importantly, these modulations of genes were differentially regulated from day one to day 21 in the cytokine combination groups.

Using IPA, we carried out an analysis to identify essential biological functions associated with cytokine combination and LPS treatments (Figure 5). IPA analysis predicted essential biological functions such as the involvement of immune cells such as macrophages, monocytes, phagocytes, neutrophils, and phagocytes. Cells were highly chemotactic, and their movement was differentially regulated from the acute to the chronic phase (Figure 5). When we investigated common genes expressed between the cytokine combination and the LPS groups, it was evident that these treatments share a 50-75% similarity. However, the number of genes expressed from the acute to the chronic conditions was not constant during individual treatments (i.e. cytokine combination and LPS) nor was their typical expression pattern (Figure 5). Most of these genes were regulated directly or indirectly through NFκB-p65 and MAPK-p38 pathways.

IPA analysis predicated that the genes directly activated by NF-κB complex at day one was VCAM1, IL-6, IL-1α, ICAM1, lipocalin (LCN)2, CCL5, and IL-4 whereas MMP3, advanced glycosylation end-product specific receptor, IL22, IL-13, CXCL6, and IL-17A were indirectly activated. Also, VEGF and SERPINE1 were inhibited (Figure S4A). Most of the genes activated were responsible for eliciting an inflammatory response. In contrast, at day 21, VCAM1, IL-6, and CCL5 were directly activated by the NF-κB complex and MMP3, CCL22, CCL11, IL-17A, and C-C motif chemokine ligand 3-like 3 were indirectly activated which were also responsible for the inflammatory response. Moreover, IGFBP2, SERPINE1, collagen type XVIII alpha 1 chain, and CX3CL1 were downregulated (Figure S4B). Compared to NFκB-p65 pathway, MAPK-p38 pathway had different degrees of response as few genes (VCAM1, IL-1α, ICAM1, MMP3, CCL5, IL-6, CSF3, IL-17A) were activated and in an indirect way on day one and day 21 (Figure S5).

Mitochondrial dysfunction and higher ROS production in MGC after cytokine combination treatment

Seahorse Mito Stress assay was performed to assess mitochondrial function in MGC upon cytokine stimulation. Oxygen consumption rate (OCR) (Figures S6B, S6E, S6H, S6K, S6N, S6Q, and S6T) and extracellular acidification rate (ECAR) (Figures S6C, S6F, S6I, S6L, S6O, S6R, and S6U) were measured with the sequential addition of oligomycin (1 uM), FCCP (2 uM), and rotenone/antimycin (0.5 uM). We observed an increase in

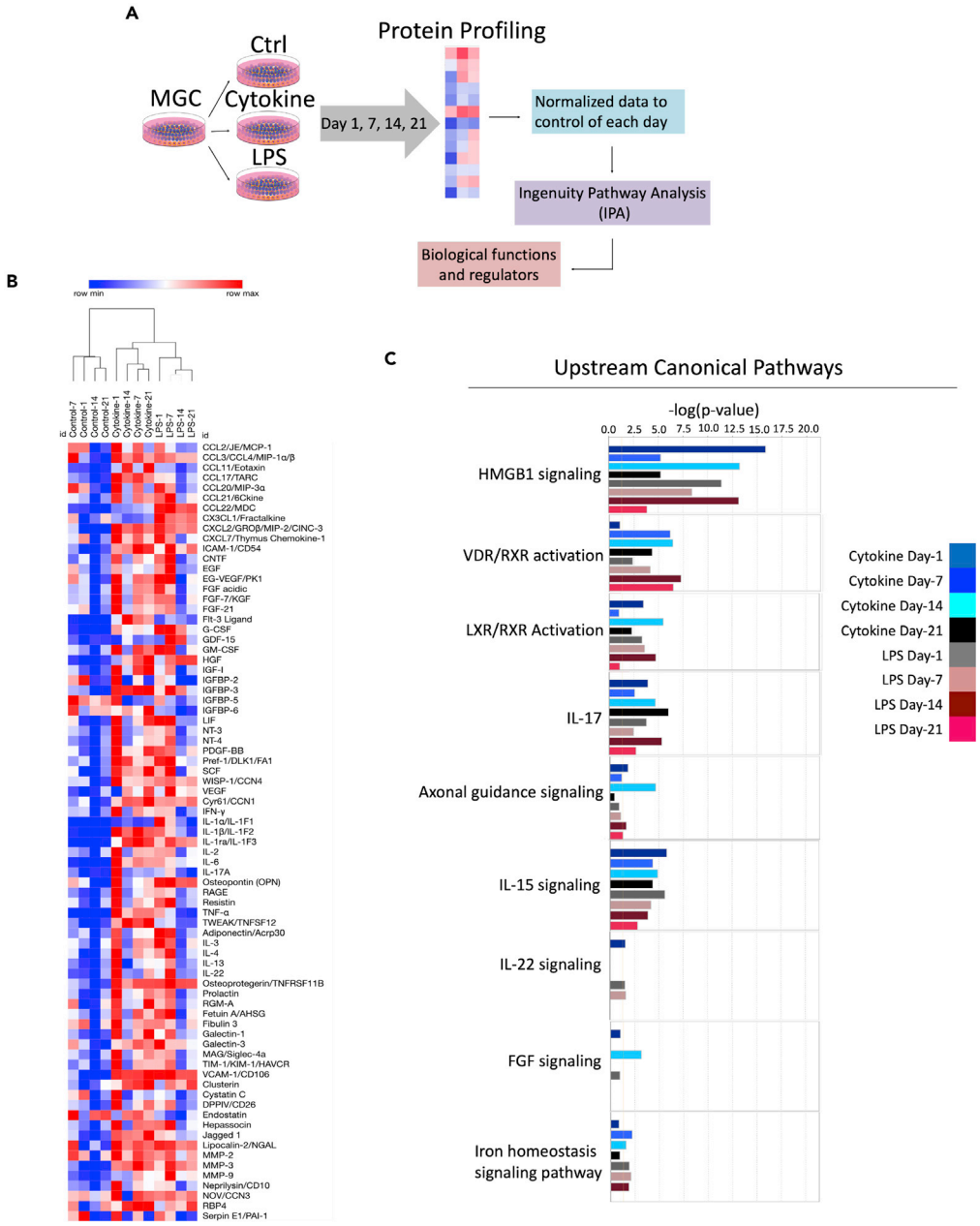

Figure 4. Differential regulation of biological functions and diseases upon cytokine induction

(A) Workflow describing steps involved in protein profiling and IPA analysis.

(B) Hierarchical clustering analysis of 79 analytes. The mean pixel density analyzed by the Proteome profile array of proteins secreted by MGC in the supernatant. Colors define activation as highly expressed (red) and no expression (blue). Only one cytokine combination (i.e. TNF-α, IL-1β, and IL-6 combination) was used along with LPS as a positive control. Treatment was given from day 1 up to day 21, and at four time points, day 1, day 7, day 14, and day 21, the supernatant was analyzed. The experiment was carried out in three biological replicates, and supernatants were pooled together, and proteome profiler array was performed. Each analyte on the array was printed in duplicate. The values shown per time point are an average of both.

(C) The upstream regulators are represented as activation *Z* score. The mean pixel density data obtained from proteome profile array were normalized to control and analyzed in IPA© software with the cutoff of 1.5 for downstream and upstream canonical pathways (See also Figures S2–S5, Data S1 and S2).

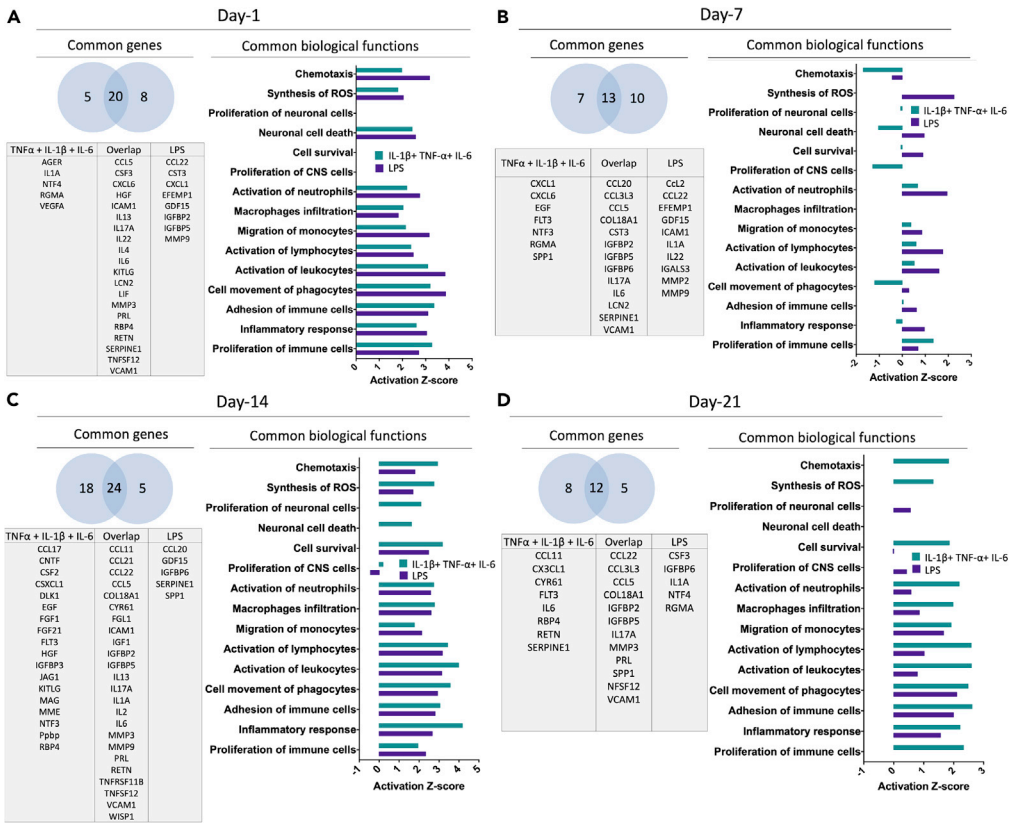

Figure 5. Transcriptome and biological function comparison between cytokine combination and LPS treatment from day one to day 21

(A, B, C, and D) Venn diagram of genes and biological functions analyzed using IPA. Genes commonly expressed between or unique in cytokine combination and LPS treatment are analyzed. Biological functions represented as activation *Z* score show positive values as upregulation, zero as no change, and negative values as downregulation (See also Data S3).

the OCR and ECAR in the cytokine treated group, which was expected as pro-inflammatory cytokines activate glial cells (Figures 6H). The cytokine group showed more acidification by glycolysis than the control group at each day of treatment (Figure 6I).

Mitochondrial activity-defining parameters were determined using OCR. The cytokine treated group showed higher maximal respiration (Figure 6C) and spare respiratory capacity (Figure 6F). The basal respiration (Figure 6B), ATP production by oxidation (Figure 6A), and its rate of production (Figure 6K) were higher in the cytokine treated group from day one to day three, but from day four to day seven, there was no difference compared to the control group. In contrast, the rate of ATP production by glycolysis was higher in the cytokine-treated groups at all time points (Figure 6J). These data correlated with the proton leak parameter, which determines whether there is mitochondrial membrane depolarization (Cheng et al., 2017). This parameter is often considered a hallmark of mitochondrial damage, which was further confirmed by calculating coupling efficiency (an efficiency to couple proton translocation across the mitochondrial membrane to ATP production), as it was lower in the cytokine-treated group (Figure 6D). In addition, cytokine combination treatment altered the ATP-induced endogenous intracellular Ca^{2+} signaling (Figure S9). Further, we used an ROS-superoxide detection kit to detect hydrogen peroxide, peroxynitrite, hydroxyl radicals, NO, and peroxy radical production in cells and found that ROS was significantly increased in the cytokine-treated MGC (Figure 6G).

High-throughput drug screening paradigm

Our proteome profile array has shown upregulation of different chemokines, and after careful analysis, we identified that among all chemokines, CINC-3 was found to be highly expressed in the cytokine treatment

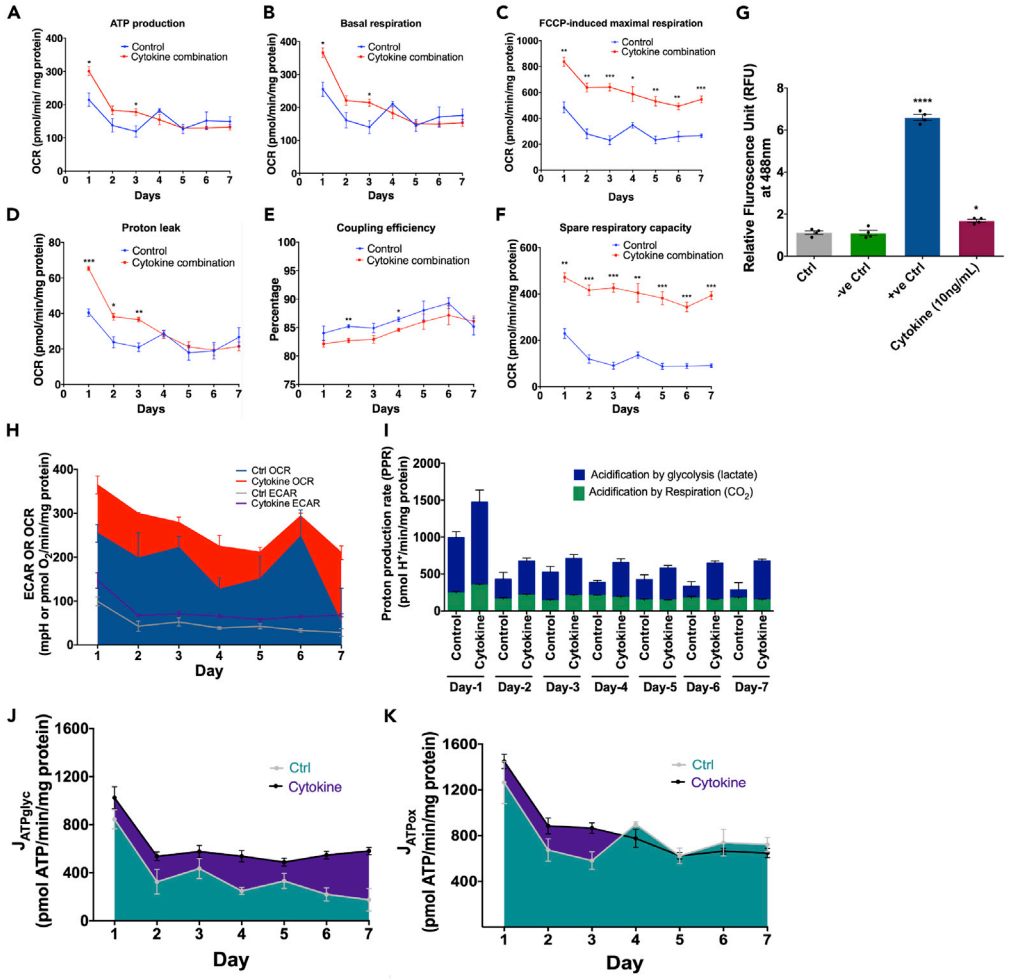

Figure 6. A cytokine combination treatment increases OCR, respiration, ATP production, and proton leak and decreases coupling efficiency and membrane potential over seven days

(A–F) All parameters were calculated as a function of a cytokine combination treatment. For this, total protein per well was calculated using a BCA protein quantification assay, and data were normalized against it. Data are represented as mean ± SEM, n = three independent experiments. *p < 0.05, **p < 0.01, ***p < 0.001 vs respective day of control. A student t-test was performed to test the difference between the treatment and the respective day of control.

(G) ROS species detected using an ROS-superoxide assay confirms an increase in the oxidative stress in MGC. Negative control (-ve Ctrl): ROS inhibitor (N-acetyl-L-cysteine), positive control (+ve Ctrl): ROS inducer (Pyocyanin). Data are represented as mean ± SEM, n = four experimental replicates, *p < 0.05, ****p < 0.001 compared with the Ctrl (control) group.

(H) Basal ECAR and OCR plotted on the same axis obtained from control and cytokine combination treatment to MGC.

(I) Rate of extracellular acidification caused by glycolysis by lactate production and respiration by CO_2 production from day one to day seven. Both control and cytokine combination treatment groups showed an increase in acidification by glycolysis rather than by respiration, whereas compared to the control, the cytokine treatment increases glycolysis-based acidification. However, there was no difference between the control and the cytokine treatment group in acidification by respiration.

(J) Data from basal ECAR and OCR have been converted to the rate of ATP production by glycolysis using formula.

(K) Data from basal ECAR and OCR have been converted to the rate of ATP production by oxidation using the formula. Data are represented as mean ± SEM, n = three experimental replicates (See also Figures S6 and S9 and Data S4).

(Figures S7 and 4C) and CINC-3 expression was thus used as a biomarker for drug screening. Upon cytokine stimulation, we found significantly high secretion of CINC-3 from glial cells from six hr to 48 hr (Figures S8A–S8F). The Z′ factor calculated to identify the assay suitability was found to be 0.96 (very high) between

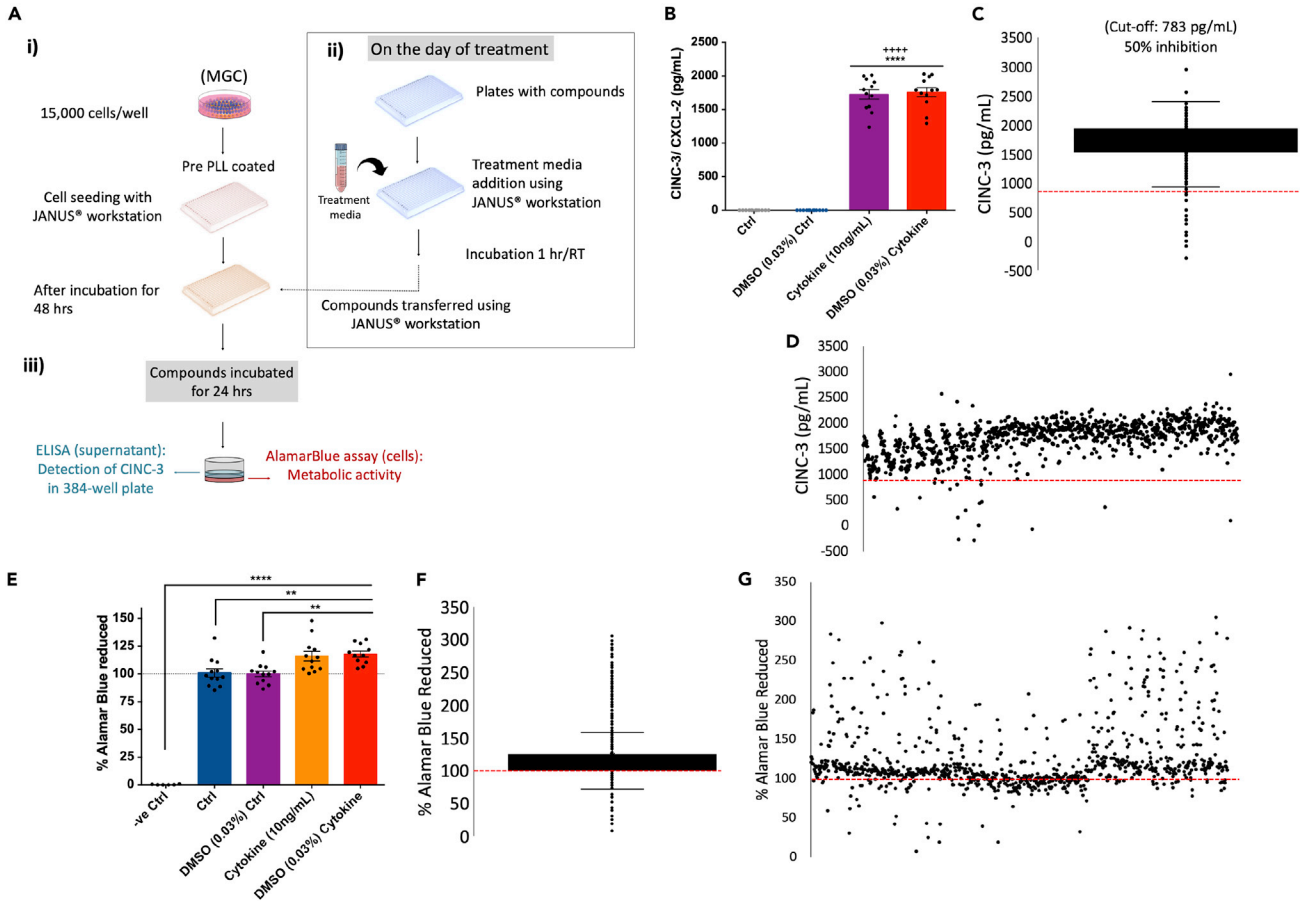

Figure 7. HTS optimization, validation, and its use to identify novel targets for inflammation

(A) Workflow for high-throughput screening. (i)15,000 cells/well/50 uL were seeded in pre-PLL-coated 384-well plates and were left to grow for two days. (ii) After two days, 50 uL of the treatment media (without FBS and with cytokine combination) was added into compound plates and incubated for an hour. The treatment media containing compounds was transferred to cell plates after removal of original media. (iii) Compounds were incubated with cells for 24 hr. Further, ELISA was performed on the supernatant to assess CINC-3 expression from each well and alamarBlue assay on cells. All the steps were carried out using a JANUS workstation. There were three compound plates, and each plate contained four replicates of controls (Ctrl, DMSO (0.03%), cytokine combination (IL-1β+ TNF-α+ IL-6, 10 ng/mL each), and DMSO + cytokine combination.

(B) Increase in the CINC-3 expression after cytokine combination treatment. Data are represented as mean ± SEM, n = 12, ****$p < 0.0001$ compared with Ctrl, $^{++++}p < 0.0001$ compared with DMSO (0.03%) Ctrl; one-way ANOVA followed by *post hoc* Tukey test.

(C) Three plates pulled assay points (box plot). Red dotted line: cutoff point (i.e. 783 pg/mL) for 50% inhibition of CINC-3.

(D) Three plates pulled assay points (scattered dot plot).

(E) alamarBlue assay showing metabolic activity after cytokine combination treatment. Red dotted line: Normalized and compared with the control (i.e. 100%). Data are represented as mean ± SEM, n = three experimental replicates with four technical replicates, ****$p < 0.0001$, **$p < 0.01$; one-way ANOVA followed by *post hoc* Tukey multiple comparison test.

(F) All assay points (box plot).

(G) All assay points (scattered dot plot) (See also Figures S7 and S8 and Table S2).

the control and the cytokine-treated group at 24 hr (Figure S8G). Therefore, we decided to use 24 hr as the biological time point to assess the anti-inflammatory effect of drugs.

We repeated the 24 hr time point for this assay using JANUS workstation and multidrop. We obtained similar results with Z′ factor of 0.79 between the control and the cytokine-treated group (Figure 7B). As described in Figure 7A, this screen was carried out in four days on a 786-compound library (Enzo Life Sciences) to screen anti-inflammatory drugs. MGC cells were seeded in plates two days *in vitro*, and then, the cytokine treatment and drug administration to cells were carried out. On the final day, CINC-3 detection and alamarBlue assay were performed. The data were analyzed, and a cutoff of 50% inhibition for

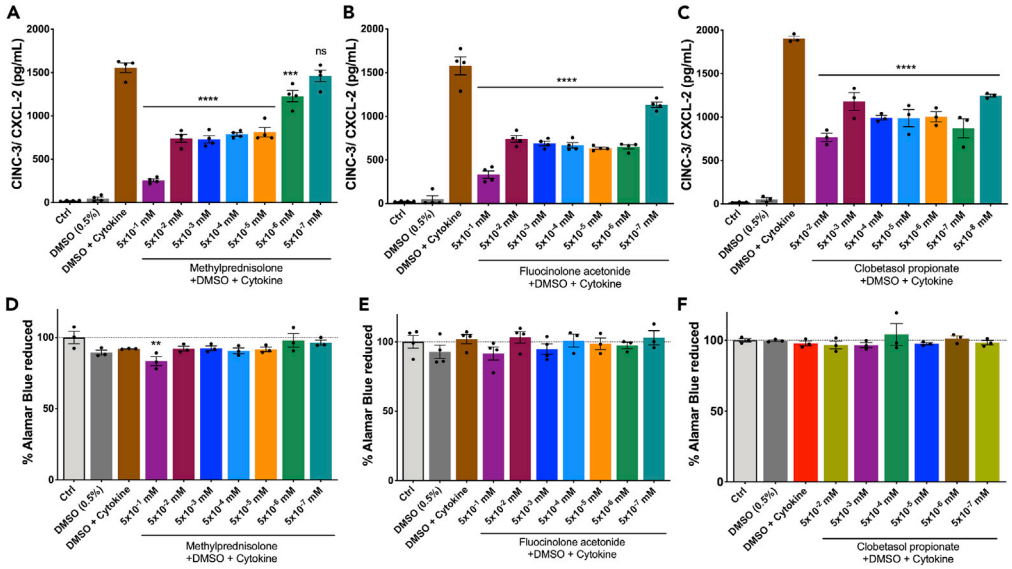

Figure 8. Validation of HTS—dose-dependent significant reduction of CINC-3 production upon corticosteroids treatment during secondary screening

(A) Methylprednisolone treatment.

(B) Fluocinolone acetonide.

(C) Clobetasol propionate treatment.

(D–F) There were no metabolic changes upon drug induction. Data are represented as mean ± SEM, n = three-four experimental replicates. For (A-C), ****$p < 0.0001$, ***$p < 0.001$ vs DMSO + cytokine group; for (D-F), **$p < 0.01$ vs Ctrl group. One-way ANOVA followed by post hoc Tukey test (See also Figure S11 and Table S2).

CINC-3 production (i.e.783 pg/mL) was applied to identify anti-inflammatory compounds (Figures 7C and 7D). The alamarBlue assay performed after ELISA showed that there was no depletion in metabolic activity upon cytokine treatment (Figure 7E) and more than 95% of drugs had no harmful effect on metabolic activity (Figures 7F and 7G). Based on the cutoff value, we obtained a primary list of the drugs (Table S2). This list contains cytotoxic, corticosteroids, anti-bacterial, and anti-fungal compounds.

We performed dose-response studies to validate the HTS platform. We assessed ELISA (CINC-3) on the supernatant collected from wells and alamarBlue assay on cells to assess metabolic activity. As expected, we showed that three of the corticosteroids, methylprednisolone, fluocinolone acetonide, and clobetasol propionate, reduced CINC-3 expression in a dose-dependent manner (Figures 8A–8C) without affecting the metabolic activity of MGC (Figures 8D–8F). Very high doses of these drugs caused cell death due to drug precipitation, as they were water insoluble (data not shown). In addition, we also confirmed the GFAP protein expression in astrocytes (in MGC) upon drug treatments along with cytokine combination. The protein levels were unaltered under these treatments (Figure S11).

DISCUSSION

The inflammation associated with SCI occurs due to activation of microglia and astrocytes (Popovich et al., 1997); this is followed by glial scar formation because of reactive astrogliosis (activation of astrocytes). These are the significant events which are responsible for the death of healthy oligodendrocytes and neurons around the lesion site, which sometimes leads to irreversible damage (Fitch and Silver, 2008). In the field, there are no appropriate well-characterized and robust *in vitro* models to study the cumulative response of astrocytes and microglia in different stages of inflammation. Here, we have established an MGC prepared from the spinal cord of postnatal rats. To the best of our knowledge, this is the first study of an *in vitro* model, which represents the acute and the chronic inflammatory state for SCI. Unlike single-cell-type screening models, in which separation of microglia and astrocytes pose another level of complexity in the procedure, this method provides a standardized and an easy way of culturing the glia and using the setup as a screening platform.

MGCs are being prepared from spinal cords, either embryonic or postnatal. Both tissue types show variability in terms of the type of cells and the percentage of them (Malon and Cao, 2016) (Beaudet et al., 2015). Here, we used postnatal three-day-old rats to culture spinal cord MGCs. The culture mostly comprises GFAP+ astrocytes and CD11b+ microglia with a small fraction of olig2+ oligodendrocytes. Due to the deliberate lack of specific growth factors and supplements in the medium, the culture was devoid of β-III tubulin + neurons. This allowed the culture to focus on only glia. The choice of using MGC instead of astrocytes or microglia alone is due to the complexity of the inflammatory process. There are reports where microglia-mediated inflammatory responses activate astrocytes via P2Y1 receptors during brain trauma (Shinozaki et al., 2017). Also, reactive microglia activate A1-type reactive astrocytes (Liddelow et al., 2017). Therefore, understanding inflammation and proposing a suitable model for a high-throughput platform needs both cell types, which was missing in most of the earlier available models (Foresti et al., 2013). The shape of astrocytes and microglia is well known to be one of the features of their activation. Astrocytes become hypertrophied as processes stained with GFAP become elongated and thicken upon activation (Cekanaviciute and Buckwalter, 2016). Previously, it has been shown that under LPS stimulation, microglial morphology changes as they become more ameboid (M1 type) in shape upon activation (Tam and Ma, 2014). These changes were similarly observed in our MGC model upon cytokine combination treatment. Based on these observations, we believe that for these characteristic shape changes, it is necessary that both glial cell types be present in direct contact with each other. Microglia response to an initial insult to the injury causes activation and chronic inflammatory stimulation leads to priming of microglia. This phenomenon is observed upon traumatic brain injury and SCI (Norden et al., 2015). Our MGC cultures comprise 45% of microglia. The primed microglia become more proliferative as we have seen in our study. Microglial priming leads to the production of pro-inflammatory cytokines and chemokines, which we have noted in our proteome profiling data. We have seen an increase in the number of microglia in culture upon cytokine combination treatment. There have been studies where microglial activation is caused by one or more of the pro-inflammatory cytokines such as TNF-alpha, IL-1beta, or IL-6. We have used a media control as a negative control and LPS as a positive control. These control groups were used as a baseline for glial activation/priming. Our studies corroborate the recent studies that have shown that primed microglia activate reactive astrocytes (Liddelow et al., 2017) (which are present in our MGC model).

One of the significant challenges in studying inflammation in the spinal cord context is understanding its acute and chronic phases. To the best of our knowledge, there are currently no models which are available to assess the behavior of astrocytes and microglia in the acute and the chronic phases. To address this mechanism, we treated MGC for 21 days, and a specific cytokine dose was given on alternate days. The choice of the alternate day was to give half a fresh media with the treatment combination. It will allow cells to have an energy source and mimic the environment where pro-inflammatory cytokines are present at the injury site. For 21 days, the impact of each pro-inflammatory cytokine on the NF-κB and MAPK pathways was studied as they are involved in the modulation of inflammation (Santa-Cecília et al., 2016) and proliferation and differentiation (Stipursky et al., 2012) of glial cells. More importantly, the levels of TNF-α, IL-1β, and IL-6 increased and peaked at an early stage (earlier than 12 hr) after SCI and remained detectable up to 120 days (Rodríguez-Barrera et al., 2020). TNF-α is known for its pleiotropic effects and is considered one of the strong mediators of the NFκB-p65 pathway (Hayden and Ghosh, 2014). Therefore, in the combinatorial cytokine treatments, the presence of TNF-α showed higher activation of this pathway at time points from day one to day ten. Its activation has a strong effect on chronic modulation of astrocytes as seen in astrocyte culture models in amyotrophic lateral sclerosis (Crosio et al., 2011). Chemokines regulate inflammatory processes through a chemokine signaling pathway that is influenced through the activation of NF-κB pathway (Richmond, 2002). We did not see the production of any anti-inflammatory cytokines or growth factors in the cytokine-treated groups, which confirms that only pro-inflammatory pathways were upregulated. Generally, growth factors are involved in regeneration processes, and during inflammation, their expression level decreases (Anderson et al., 2018). Moreover, we observed upregulation of galectin-3, ICAM-1, and VCAM-1 (glycoproteins) in treated groups which are known to participate in the inflammation process (Rabinovich and Toscano, 2009). We observed a second peak of the activation of NFκB-p65 and p38-MAPK pathway at day 10 and 13, respectively, which is a sign of reactivation of microglia. There is evidence that in SCI, during inflammatory phase, microglia adopt a mixture of M1 (classical activation) and M2 (alternate activation). It has been reported that after primary activation of microglia in the first three to seven days after injury, they reactivated again at around 14 days after injury (Akhmetzyanova et al., 2019) (Bellver-Landete et al., 2019) (Kigerl et al., 2009). Moreover, continuous inflammatory stimulation can contribute to a second phasic immune response, with the predominance of the M1 phenotype

(Akhmetzyanova et al., 2019). As mentioned before, microglial activation leads to changes in astrocyte phenotypes/functions and with the second phasic response can lead to further astrocyte activation causing higher activation of them. As explained above, the regulations of these transformations of glia are controlled by canonical pathways including NF-κB and MAPK pathways. In our proteome profiling, we confirm these findings as we observed the second wave of activation of inflammatory pathway modulators at day 14, which correlates with the timeline.

The IPA regulator network analysis predicated few biological functions such as the involvement of macrophages, monocytes, phagocytes, neutrophils, and phagocytes. This can be correlated with the SCI *in vivo* data, which reported that after the injury, these immune cells reach the site of injury and play a critical role in the activation of glial cells (Trivedi et al., 2006). As microglia are resident macrophages of the central nervous system, many molecules secreted by activated microglia may have a similarity with the secretome of immune cell types. It can also be predicted that from day one and day seven, the cytokine-treated group had a favorable condition for glial proliferation, which also support the findings of higher OCR, ECAR, and glycolysis upon cytokine induction. We observed that the NF-κB and MAPK pathway differentially regulated chemokines, cytokines, growth factors, MMPs, and glycoproteins under cytokine treatment from the acute to the chronic phase of inflammation. This was further confirmed as our IPA regulator network analysis also predicted the same pattern of activation.

Moreover, the molecules controlled by this pathway were also responsible for the induction of an inflammatory response. Day one showed high activation of the NF-κB complex and higher neuroinflammatory response, whereas on day 21, this was decreased. This pathway had either a direct or indirect effect of critical regulators responsible for inflammation, whereas MAPK pathway indirectly regulated neuroinflammatory response at day one and day 21 by regulating few genes. Changes in the expression of proteins had a significant effect on several inflammatory conditions which mimic modulations observed during different stages of SCI. This includes chemotaxis, death of healthy neurons, and infiltration of macrophages, monocytes, leukocytes, and lymphocytes, and synthesis of ROS. Surprisingly, we observed that even though cytokine combination treatments were given every alternate day, none of them kept the pathway activated for a long time.

Upon analyzing upstream regulators, we found PTEN was downregulated. It is a negative regulator of PI3/AKT/mTOR pathway (Chen et al., 2016). Activation of PI3/AKT/mTOR pathway is necessary in glial scar formation (Luan et al., 2017). PTEN has several downstream effects such as cellular growth cycle tuning and limiting uncontrolled cell growth (Rafalski and Brunet, 2011). In our experimental setup, we observed a higher metabolic rate and associated higher proliferation of glia, particularly microglia, after the cytokine combination treatment. This supports our finding of upregulation of mTOR and downregulation of PTEN. Also, suppressor of cytokine signaling 3 which negatively controls the cytokine mediated inflammation (Okada et al., 2006) is also downregulated.

We also assessed the functionality of mitochondrial activity during inflammation. It has been well reported that under inflammation stimuli (Joshi et al., 2019) or several pathological conditions (Hou et al., 2019), mitochondrial changes will have severe impacts on alleviating the disease conditions. The OCR is the direct measurement of mitochondrial electron transport rate, and ECAR is proportional to the metabolic activity of the cells. Therefore, an increase in the ECAR can be correlated with higher metabolic activity. This is typically measured by detecting lactate production. At neutral pH, when glucose is converted to lactate, it releases protons during glycolysis making medium acidic by the formation of carboxylate anion. Measurement of this provides a direct and quantitative glycolytic rate. During cytokine combination treatment, astrocytes and microglia become reactive, especially microglial rate of proliferation, which increases drastically. This subsequently increases glycolysis as there is a high demand for ATP, causing increased mitochondrial activity and an increased OCR. In this study, we observed that a cytokine combination treatment caused an increase in oxidative phosphorylation and ATP production from day one to day three. Mitochondrial basal respiration and linked ATP production also reduced after the fourth day until day seven. During cytokine combination treatment, glial metabolism increases and so does the glucose consumption. It is well known that immune cells with quiescent and anti-inflammatory phenotype primarily rely on fatty acid metabolism, whereas pro-inflammatory phenotypic immune cells use glycolysis as the main source of ATP production (Nonnenmacher and Hiller, 2018). This increases lactate production via glycolysis and CO_2 production via mitochondrial oxidative phosphorylation (respiration) which acidifies the medium.

Using OCR and ECAR values, we calculated the proton production rate and found that acidification by the glycolysis process was higher than acidification by respiration. Inflammation triggered in MGC caused mitochondrial respiration impairment as proton leak was increased and coupling efficiency was decreased from day one to day seven. This was caused by a greater number of cells losing mitochondrial membrane potential upon cytokine combination treatment. Due to the imbalance between energy need and the capacity of mitochondria, there is leakage of protons from the inner membrane of mitochondria. In the end, this leads to the production of ROS (Visavadiya et al., 2016) which can persist for weeks to months after SCI (Donnelly and Popovich, 2008). According our observation to IPA prediction showed ROS was prevalent during chronic condition upon cytokine induction in MGC.

In proteome profiling, one of the chemokines, CINC-3, which belongs to the family of CXC chemokine (Shibata et al., 2000) was found to be increased after cytokine treatment. It plays the role of chemoattractants in immune responses. CINC-3 has been well studied in rat models (Takano and Nakagawa, 2001) in inflammatory conditions. CINC-3 has a role in neutrophil requirement at the site of injury; however, it has never been used to test inflammation in MGC. Also, it has never been used as a biomarker for drug screening. Therefore, we decided to further validate the production of CINC-3 during cytokine treatment and found that there was a significant increase after the treatment. We confirmed that this assay is with huge potential as Z′ factor value was close to '1' and our assay reflects in the category of 'Ideal assay'. We further successfully demonstrated the low volume 384-well plate ELISA method-based detection of CINC-3. Here, we used only 20-30 μL of testing volume and antibody volume, which provides venture for new highly sensitive small volume setup for HTS. This could be performed either manually or by using specialized robotic liquid handling systems. Selected glucocorticosteroids for secondary screening are often used for their immunosuppressant and anti-inflammatory activity which brings their mode of action by inhibiting classical NFkB-p65 pathway (Yasir et al., 2020). This further would have inhibited CINC-3 production as its production is controlled by key gene regulator NF-κB (Takaishi et al., 2000). Additionally, upregulation in the GFAP expression which is considered an hallmark for reactive astrocytes (Liddelow and Barres, 2017). However, when we assessed the changes in GFAP protein levels in cytokine combination treatment and glucocorticosteroid-treated groups, we did not see any change. This outcome was comparable with the reported data which showed that at *in vitro* level upon cytokine (TNF-α and or IL-1β) treatment, the GFAP expression was reduced instead of increased in *in vitro* models (Hyvärinen et al., 2019).

In conclusion, treatment with cytokine combinations successfully induced acute and chronic-like inflammatory conditions in MGC associated with SCI at the preclinical level. This model addresses limitations of current *in vitro* models of SCI. Pro-inflammatory cytokine combination treatments showed that different cytokines influenced the different level of expression of neuroinflammatory pathways. From the acute to the chronic phases, NF-κB and MAPK gene regulators showed variable effects on the modulation of pro-inflammatory milieu. One can use this approach to investigate future treatments and conduct screenings to evaluate drug or molecule's efficacy before proceeding for preclinical studies. Importantly, this platform can be used to screen therapeutic interventions for neuroinflammatory diseases, including SCI using high-throughput platforms.

Limitations of the study

One of the limitations of the study is that, as several factors influence the glial cells, further studies would be needed to encompass the entire complexity of SCI. For example, future models should take into consideration the response of myelin debris or blood-born immune cells for reliable drug testing for the respective mode of action.

Resource availability

Lead contact

Further information and requests for resources should be directed to and will be fulfilled by the lead contact, Abhay Pandit (abhay.pandit@nuigalway.ie).

Material availability

This study did not generate new unique reagents.

Data and code availability

All data supporting the results can be found in this manuscript and as Supplemental information. Data requests can be addressed to the corresponding author.

ETHICS STATEMENT

In this study, we used female Sprague-Dawley rats (Charles River UK Ltd., Margate, UK). All housing and procedures carried out in this study were approved by the Animal Care Research Ethics Committee (ACREC) at the National University of Ireland, Galway.

METHODS

All methods can be found in the accompanying Transparent methods supplemental file.

SUPPLEMENTAL INFORMATION

Supplemental information can be found online at https://doi.org/10.1016/j.isci.2021.102182.

ACKNOWLEDGMENTS

We would like to thank Dr Raghvendra Bohara and Anthony Slone for editing the manuscript and Dr Sukharaj Dhami for assistance in flow cytometry. The authors acknowledge the facilities and scientific and technical assistance of the Centre for Microscopy & Imaging at the National University of Ireland Galway (www.imaging.nuigalway.ie). We are grateful to the facilities and scientific and technical assistance of the Genomics and Screening and Flow Cytometry Core at the National University of Ireland Galway, a facility that is funded by the Science Foundation Ireland, National University of Ireland, Galway and the Irish Government's Programme for Research in Third Level Institutions, Cycles 4 and 5, National Development Plan 2007-2013, and the European Regional Development Fund. This publication has emanated from research supported in part by a grant from the Science Foundation Ireland and is co-funded under the European Regional Development Fund under grant number 13/RC/2073 and 13/RC/2073_P2.

AUTHOR CONTRIBUTIONS

V.P. designed the study, performed all the experiments, analyzed and interpreted the data, and wrote the paper. E.O. and H.F. contributed to the HTS data acquisition. H.F. made available the Enzo screening library. L.Q. provided electrophysiology facility to perform calcium imaging and contributed in analysis of the calcium imaging data. S.M. contributed to data analysis and interpretation. All authors were involved in the drafting or critical revision of the article and approved the final version. A.P. contributed to the concept, data analysis, interpretation, had full access to all the data in the study, and took responsibility for the integrity of the data and accuracy of the conclusions.

DECLARATION OF INTERESTS

The lead author declares that the invention disclosure form (IDF) is filled entitled "Designing of *In vitro* Inflammatory Model for High Throughput Drug Screening".

Received: July 27, 2020
Revised: December 25, 2020
Accepted: February 9, 2021
Published: March 19, 2021

REFERENCES

Akhmetzyanova, E., Kletenkov, K., Mukhamedshina, Y., and Rizvanov, A. (2019). Different approaches to modulation of microglia phenotypes after spinal cord injury. Front. Syst. Neurosci. *13*, 1–12.

Alizadeh, A., Dyck, S.M., and Karimi-Abdolrezaee, S. (2019). Traumatic spinal cord injury: an overview of pathophysiology, models and acute injury mechanisms. Front. Neurol. *10*, 282.

Anderson, M.A., O'Shea, T.M., Burda, J.E., Ao, Y., Barlatey, S.L., Bernstein, A.M., Kim, J.H., James, N.D., Rogers, A., Kato, B., et al. (2018). Required growth facilitators propel axon regeneration across complete spinal cord injury. Nature *561*, 396–400.

Beaudet, M.-J., Yang, Q., Cadau, S., Blais, M., Bellenfant, S., Gros-Louis, F., and Berthod, F. (2015). High yield extraction of pure spinal motor neurons, astrocytes and microglia from single embryo and adult mouse spinal cord. Sci. Rep. *5*, 16763.

Becher, B., Spath, S., and Goverman, J. (2017). Cytokine networks in neuroinflammation. Nat. Rev. Immunol. *17*, 49–59.

Bellver-Landete, V., Bretheau, F., Mailhot, B., Vallières, N., Lessard, M., Janelle, M.-E., Vernoux, N., Tremblay, M.-È., Fuehrmann, T., Shoichet, M.S., and Lacroix, S. (2019). Microglia are an

essential component of the neuroprotective scar that forms after spinal cord injury. Nat. Commun. *10*, 518.

Cekanaviciute, E., and Buckwalter, M.S. (2016). Astrocytes: Integrative regulators of neuroinflammation in stroke and other neurological diseases. Neurotherapeutics *13*, 685–701.

Chen, C.-H., Sung, C.-S., Huang, S.-Y., Feng, C.-W., Hung, H.-C., Yang, S.-N., Chen, N.-F., Tai, M.-H., Wen, Z.-H., and Chen, W.-F. (2016). The role of the pi3k/akt/mtor pathway in glial scar formation following spinal cord injury. Exp. Neurol. *278*, 27–41.

Cheng, J., Nanayakkara, G., Shao, Y., Cueto, R., Wang, L., Yang, W.Y., Tian, Y., Wang, H., and Yang, X. (2017). Mitochondrial proton leak plays a critical role in pathogenesis of cardiovascular diseases. In Mito. Dyn. Cardi. Med., G. Santulli, ed. (Springer International Publishing), pp. 359–370.

Chio, J.C.T., Wang, J., Badner, A., Hong, J., Surendran, V., and Fehlings, M.G. (2019). The effects of human immunoglobulin g on enhancing tissue protection and neurobehavioral recovery after traumatic cervical spinal cord injury are mediated through the neurovascular unit. J. Neuroinflammation *16*, 141.

Crosio, C., Valle, C., Casciati, A., Iaccarino, C., and Carrì, M.T. (2011). Astroglial inhibition of nf-κb does not ameliorate disease onset and progression in a mouse model for amyotrophic lateral sclerosis (als). PLoS One *6*, e17187.

DiSabato, D.J., Quan, N., and Godbout, J.P. (2016). Neuroinflammation: the devil is in the details. J. Neurochem. *139* (*Suppl 2*), 136–153.

Donnelly, D.J., and Popovich, P.G. (2008). Inflammation and its role in neuroprotection, axonal regeneration and functional recovery after spinal cord injury. Exp. Neurol. *209*, 378–388.

Fitch, M.T., and Silver, J. (2008). Cns injury, glial scars, and inflammation: Inhibitory extracellular matrices and regeneration failure. Exp. Neurol. *209*, 294–301.

Foresti, R., Bains, S.K., Pitchumony, T.S., de Castro Brás, L.E., Drago, F., Dubois-Randé, J.-L., Bucolo, C., and Motterlini, R. (2013). Small molecule activators of the nrf2-ho-1 antioxidant axis modulate heme metabolism and inflammation in bv2 microglia cells. Pharmacol. Res. *76*, 132–148.

Gingras, M., Gagnon, V., Minotti, S., Durham, H.D., and Berthod, F. (2007). Optimized protocols for isolation of primary motor neurons, astrocytes and microglia from embryonic mouse spinal cord. J. Neurosci. Methods *163*, 111–118.

Hayden, M.S., and Ghosh, S. (2014). Regulation of nf-κb by tnf family cytokines. Semin. Immunol. *26*, 253–266.

Hou, Y., Dan, X., Babbar, M., Wei, Y., Hasselbalch, S.G., Croteau, D.L., and Bohr, V.A. (2019). Ageing as a risk factor for neurodegenerative disease. Nat. Rev. Neurol. *15*, 565–581.

Hyvärinen, T., Hagman, S., Ristola, M., Sukki, L., Veijula, K., Kreutzer, J., Kallio, P., and Narkilahti, S. (2019). Co-stimulation with il-1β and tnf-α induces an inflammatory reactive astrocyte phenotype with neurosupportive characteristics in a human pluripotent stem cell model system. Sci. Rep. *9*, 16944.

Jhang, J.J., Lu, C.C., Ho, C.Y., Cheng, Y.T., and Yen, G.C. (2015). Protective effects of catechin against monosodium urate-induced inflammation through the modulation of nlrp3 inflammasome activation. J. Agric. Food Chem. *63*, 7343–7352.

Joshi, A.U., Minhas, P.S., Liddelow, S.A., Haileselassie, B., Andreasson, K.I., Dorn, G.W., and Mochly-Rosen, D. (2019). Fragmented mitochondria released from microglia trigger a1 astrocytic response and propagate inflammatory neurodegeneration. Nat. Neurosci. *22*, 1635–1648.

Kabu, S., Gao, Y., Kwon, B.K., and Labhasetwar, V. (2015). Drug delivery, cell-based therapies, and tissue engineering approaches for spinal cord injury. J. Controll. Release *219*, 141–154.

Kigerl, K.A., Gensel, J.C., Ankeny, D.P., Alexander, J.K., Donnelly, D.J., and Popovich, P.G. (2009). Identification of two distinct macrophage subsets with divergent effects causing either neurotoxicity or regeneration in the injured mouse spinal cord. J. Neurosci. *29*, 13435–13444.

Liddelow, S.A., and Barres, B.A. (2017). Reactive astrocytes: production, function, and therapeutic potential. Immunity *46*, 957–967.

Liddelow, S.A., Guttenplan, K.A., Clarke, L.E., Bennett, F.C., Bohlen, C.J., Schirmer, L., Bennett, M.L., Munch, A.E., Chung, W.S., Peterson, T.C., et al. (2017). Neurotoxic reactive astrocytes are induced by activated microglia. Nature *541*, 481–487.

Liu, W., Tang, Y., and Feng, J. (2011). Cross talk between activation of microglia and astrocytes in pathological conditions in the central nervous system. Life Sci. *89*, 141–146.

Luan, Y., Chen, M., and Zhou, L. (2017). Mir-17 targets pten and facilitates glial scar formation after spinal cord injuries via the pi3k/akt/mtor pathway. Brain Res. Bullet. *128*, 68–75.

Malon, J.T., and Cao, L. (2016). Preparation of primary mixed glial cultures from adult mouse spinal cord tissue. J. Vis. Exp. *117*, 54801.

Möller, T., and Boddeke, H.W. (2016). Glial cells as drug targets: what does it take? Glia *64*, 1742–1754.

Mutemberezi, V., Buisseret, B., Masquelier, J., Guillemot-Legris, O., Alhouayek, M., and Muccioli, G.G. (2018). Oxysterol levels and metabolism in the course of neuroinflammation: Insights from in vitro and in vivo models. J. Neuroinflammation *15*, 74.

Nonnenmacher, Y., and Hiller, K. (2018). Biochemistry of proinflammatory macrophage activation. Cell. Mol. Life Sci. *75*, 2093–2109.

Norden, D.M., Muccigrosso, M.M., and Godbout, J.P. (2015). Microglial priming and enhanced reactivity to secondary insult in aging, and traumatic cns injury, and neurodegenerative disease. Neuropharma *96*, 29–41.

Norenberg, M.D., Smith, J., and Marcillo, A. (2004). The pathology of human spinal cord injury: defining the problems. J. Neurotrauma *21*, 429–440.

Okada, S., Nakamura, M., Katoh, H., Miyao, T., Shimazaki, T., Ishii, K., Yamane, J., Yoshimura, A., Iwamoto, Y., Toyama, Y., and Okano, H. (2006). Conditional ablation of stat3 or socs3 discloses a dual role for reactive astrocytes after spinal cord injury. Nat. Med. *12*, 829–834.

Park, J.B. (2017). In silico screening and in vitro activity measurement of javamide analogues as potential p38 mapk inhibitors. Int. J. Mol. Sci. *18*, 2704.

Pineau, I., and Lacroix, S. (2007). Proinflammatory cytokine synthesis in the injured mouse spinal cord: Multiphasic expression pattern and identification of the cell types involved. J. Comp. Neurol. *500*, 267–285.

Popovich, P.G., Wei, P., and Stokes, B.T. (1997). Cellular inflammatory response after spinal cord injury in sprague-dawley and lewis rats. J. Comp. Neurol. *377*, 443–464.

Rabinovich, G.A., and Toscano, M.A. (2009). Turning 'sweet' on immunity: galectin-glycan interactions in immune tolerance and inflammation. Nat. Rev. Immunol. *9*, 338–352.

Rafalski, V.A., and Brunet, A. (2011). Energy metabolism in adult neural stem cell fate. Prog. Neurobiol. *93*, 182–203.

Richmond, A. (2002). Nf-kappa b, chemokine gene transcription and tumour growth. Nat. Rev. Immunol. *2*, 664–674.

Rodríguez-Barrera, R., Flores-Romero, A., García, E., Fernández-Presas, A.M., Incontri-Abraham, D., Navarro-Torres, L., García-Sánchez, J., Juárez-Vignon Whaley, J.J., Madrazo, I., and Ibarra, A. (2020). Immunization with neural-derived peptides increases neurogenesis in rats with chronic spinal cord injury. CNS. Neurosci. Ther. *26*, 650–658.

Santa-Cecília, F.V., Socias, B., Ouidja, M.O., Sepulveda-Diaz, J.E., Acuña, L., Silva, R.L., Michel, P.P., Del-Bel, E., Cunha, T.M., and Raisman-Vozari, R. (2016). Doxycycline suppresses microglial activation by inhibiting the p38 mapk and nf-kb signaling pathways. Neurotox. Res. *29*, 447–459.

Shibata, F., Konishi, K., and Nakagawa, H. (2000). Identification of a common receptor for three types of rat cytokine-induced neutrophil chemoattractants (cincs). Cytokine *12*, 1368–1373.

Shinozaki, Y., Shibata, K., Yoshida, K., Shigetomi, E., Gachet, C., Ikenaka, K., Tanaka, K.F., and Koizumi, S. (2017). Transformation of astrocytes to a neuroprotective phenotype by microglia via p2y1 receptor downregulation. Cell. Rep. *19*, 1151–1164.

Stipursky, J., Francis, D., and Gomes, F.C.A. (2012). Activation of mapk/pi3k/smad pathways by tgf-β_1 controls differentiation of radial glia into astrocytes in vitro. Develop. Neurosci. *34*, 68–81.

Sun, L., Li, M., Ma, X., Zhang, L., Song, J., Lv, C., and He, Y. (2019). Inhibiting high mobility group box-1 reduces early spinal cord edema and attenuates astrocyte activation and aquaporin-4 expression after spinal cord injury in rats. J. Neurotrauma *36*, 421–435.

Takaishi, K., Ohtsuka, T., Tsuneyoshi, S., Maehara, N., Harada, M., Yoshida, H., Watanabe, K., and Tsurufuji, S. (2000). Inhibition of the production of rat cytokine-induced neutrophil chemoattractant (cinc)-1, a member of the interleukin-8 family, by adenovirus-mediated overexpression of iκbα. J. Biochem. *127*, 511–516.

Takano, K., and Nakagawa, H. (2001). Contribution of cytokine-induced neutrophil chemoattractant cinc-2 and cinc-3 to neutrophil recruitment in lipopolysaccharide-induced inflammation in rats. Inflamm. Res. *50*, 503–508.

Tam, W.Y., and Ma, C.H.E. (2014). Bipolar/rod-shaped microglia are proliferating microglia with distinct m1/m2 phenotypes. Sci. Rep. *4*, 7279.

Trivedi, A., Olivas, A.D., and Noble-Haeusslein, L.J. (2006). Inflammation and spinal cord injury: Infiltrating leukocytes as determinants of injury and repair processes. Clinic. Neurosci. Res. *6*, 283–292.

Visavadiya, N.P., Patel, S.P., VanRooyen, J.L., Sullivan, P.G., and Rabchevsky, A.G. (2016). Cellular and subcellular oxidative stress parameters following severe spinal cord injury. Redox Biol. *8*, 59–67.

Wang, J., Chen, J., Jin, H., Lin, D., Chen, Y., Chen, X., Wang, B., Hu, S., Wu, Y., Wu, Y., et al. (2019). Brd4 inhibition attenuates inflammatory response in microglia and facilitates recovery after spinal cord injury in rats. J. Cell. Mol. Med. *23*, 3214–3223.

Xu, W., Chi, L., Xu, R., Ke, Y., Luo, C., Cai, J., Qiu, M., Gozal, D., and Liu, R. (2005). Increased production of reactive oxygen species contributes to motor neuron death in a compression mouse model of spinal cord injury. Spinal Cord *43*, 204–213.

Yasir, M., Goyal, A., Bansal, P., and Sonthalia, S. (2020). Corticosteroid Adverse Effects. *Statpearls* (StatPearls Publishing Copyright © 2020, StatPearls Publishing LLC).

Zhang, C., Li, C., Jia, X., Wang, K., Tu, Y., Wang, R., Liu, K., Lu, T., and He, C. (2019). In vitro and in vivo anti-inflammatory effects of polyphyllin vii through downregulating mapk and nf-κb pathways. Molecules *24*, 875.

iScience, Volume *24*

Supplemental information

A robust platform for high-throughput screening of therapeutic strategies for acute and chronic spinal cord injury

Vaibhav Patil, Enda O'Connell, Leo R. Quinlan, Howard Fearnhead, Siobhan McMahon, and Abhay Pandit

Supplemental Information

Table S1: Groups of cytokine combination treatments for 21 days study. Related to Figure 3.

Ctrl: Control, M-Ctrl: Media control. All used with 10 ng/mL of dose.

	TNF-α	IL-1β	IL-6	LPS	Time (Days)
1	+	-	-	-	1-21
2	-	+	-	-	-//-
3	-	-	+	-	-//-
4	+	+	-	-	-//-
5	-	+	+	-	-//-
6	+	-	+	-	-//-
7	+	+	+	-	-//-
8	-	-	-	+	-//-
9	Ctrl	Ctrl	Ctrl	-	-//-
10	M-Ctrl	M-Ctrl	M-Ctrl	-	-//-

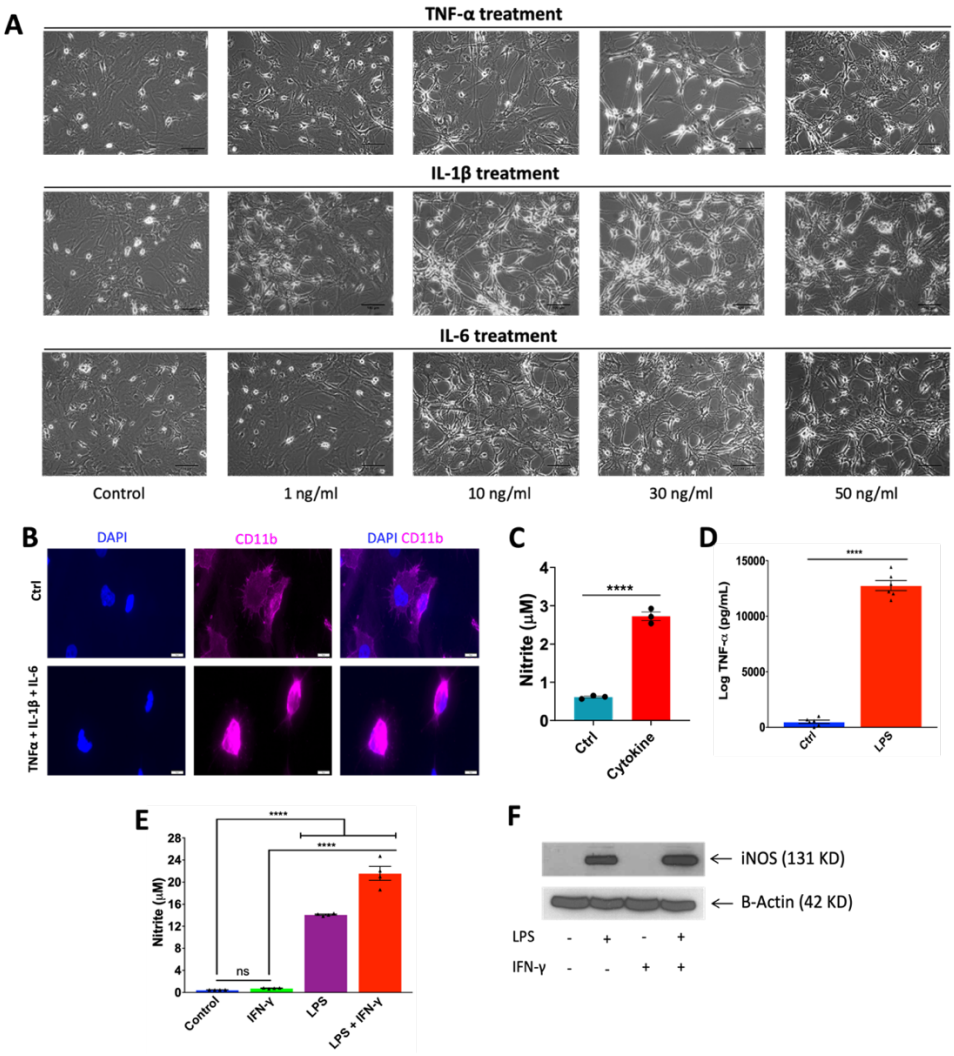

Figure S1: The cytokine combination treatment induces morphological changes in MGC. Related to Figure 2.

(A) Individual treatment of TNF-α, IL-1β and IL-6 with the concentration of 1, 10, 30 and 50 ng/mL showed morphological changes in MGC. Scale bar=100 µm. (B) Morphological changes in microglia as they became more ameboid shape upon cytokine combination treatment. Scale bar= 10 µm. (C) Griess assay showing the effect of cytokine combination (cytokine) on nitrite production. Data are expressed as mean ± SEM, n=three independent experiments with two technical replicates; $^{****}p<0.0001$, student *t*-test. (D) TNF-α expression after lipopolysaccharide (LPS) treatment. Data are expressed as mean ± SEM, n=three independent experiments with two technical replicates; $^{****}p<0.0001$, student *t*-test. (E) Griess assay showing the effect of LPS (100 ng/mL) and IFN-γ (10 ng/mL) on nitrite production. Data is expressed as mean ± SEM, n= two independent experiments with four technical replicates; $^{***}p<0.001$, $^{*}p<0.05$, one-way analysis of variance (ANOVA), post hoc Tukey test. (F) Western blot showing expression of iNOS upon treatment of LPS and LPS + interferon (IFN)-γ. Based upon these results, 100 ng/mL dose of LPS was selected for further studies.

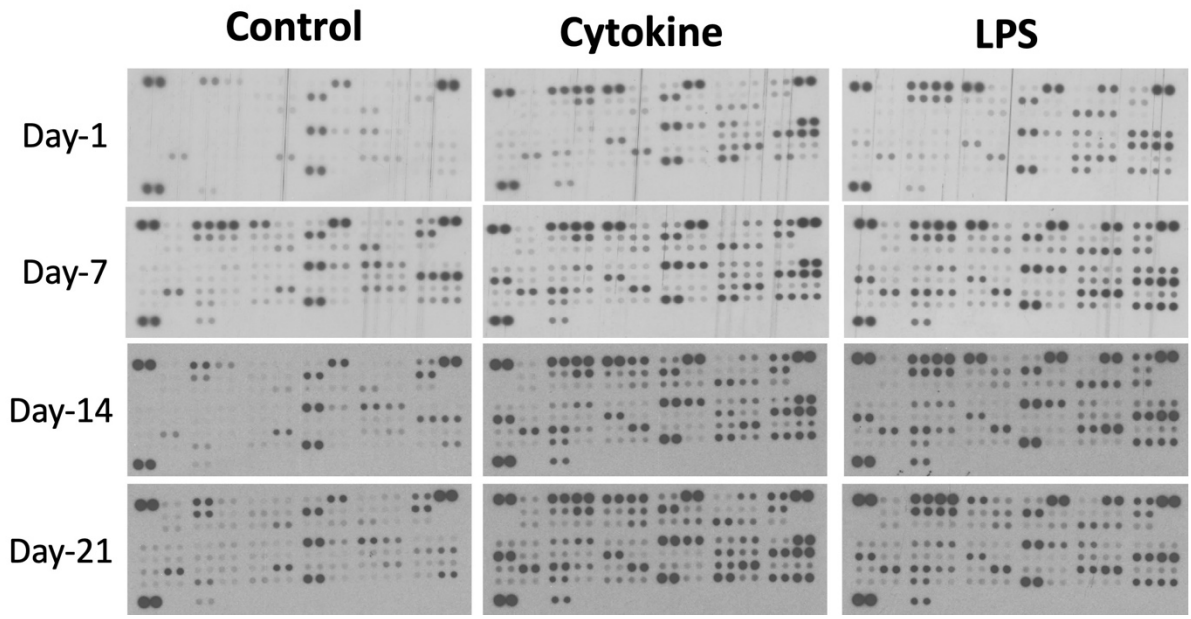

Figure S2: The Rat XL Cytokine Array detects multiple cytokines, chemokines, growth factors and other soluble proteins in the media (supernatant). Related to Figure 4.

Twelve blots for four time points (day-1, day-7, day-14 and day-21) and three conditions (Control, cytokine combination (10 ng/mL of each cytokine), and LPS (100 ng/mL)). Three experimental replicates pulled supernatant (media) run for two technical replicates (as each analyte was in duplicate).

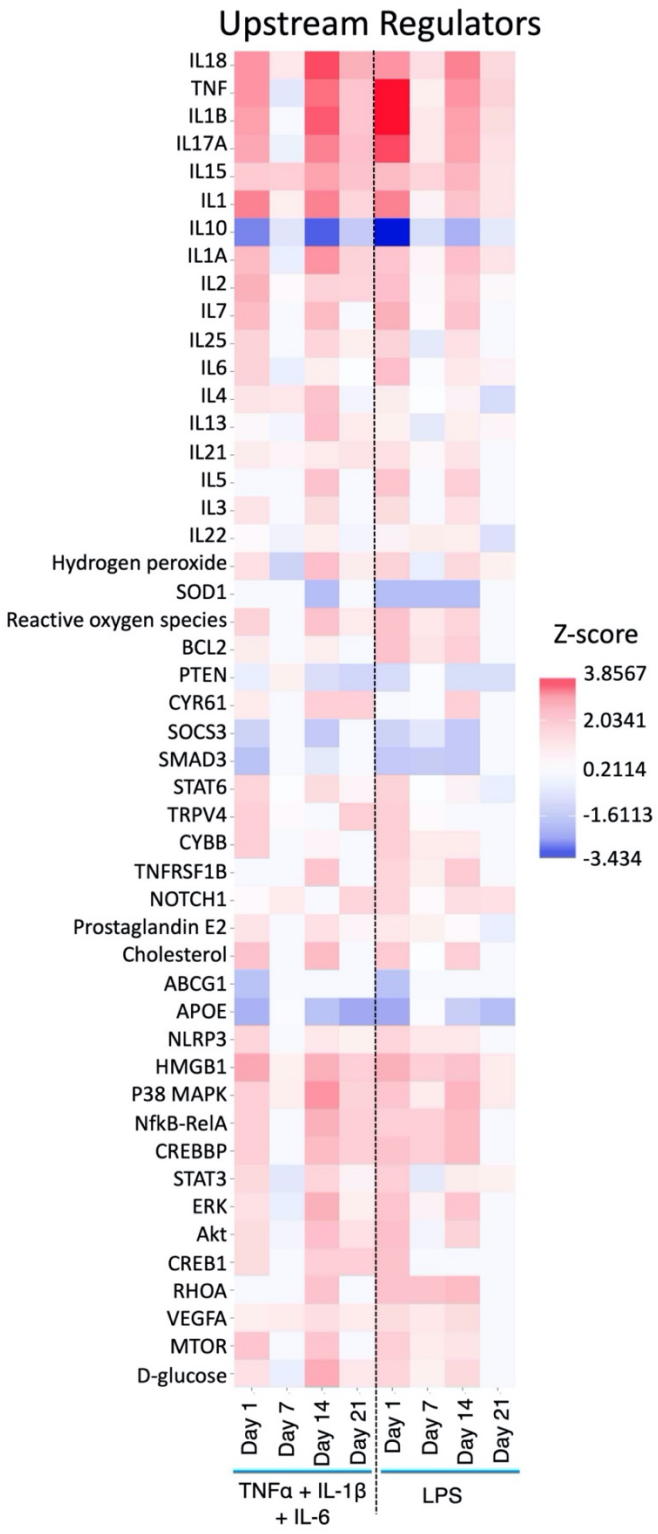

Figure S3: Differential regulation of upstream regulators upon cytokine and LPS induction. Related to Figure 4 and see also Data S2.

The mean pixel density data obtained from the proteome profile™ array was normalised to control and analysed in Ingenuity Pathway Analysis (IPA)© software with the cut-off of 1.5 for downstream and upstream regulators. The data are represented as activation Z-score.

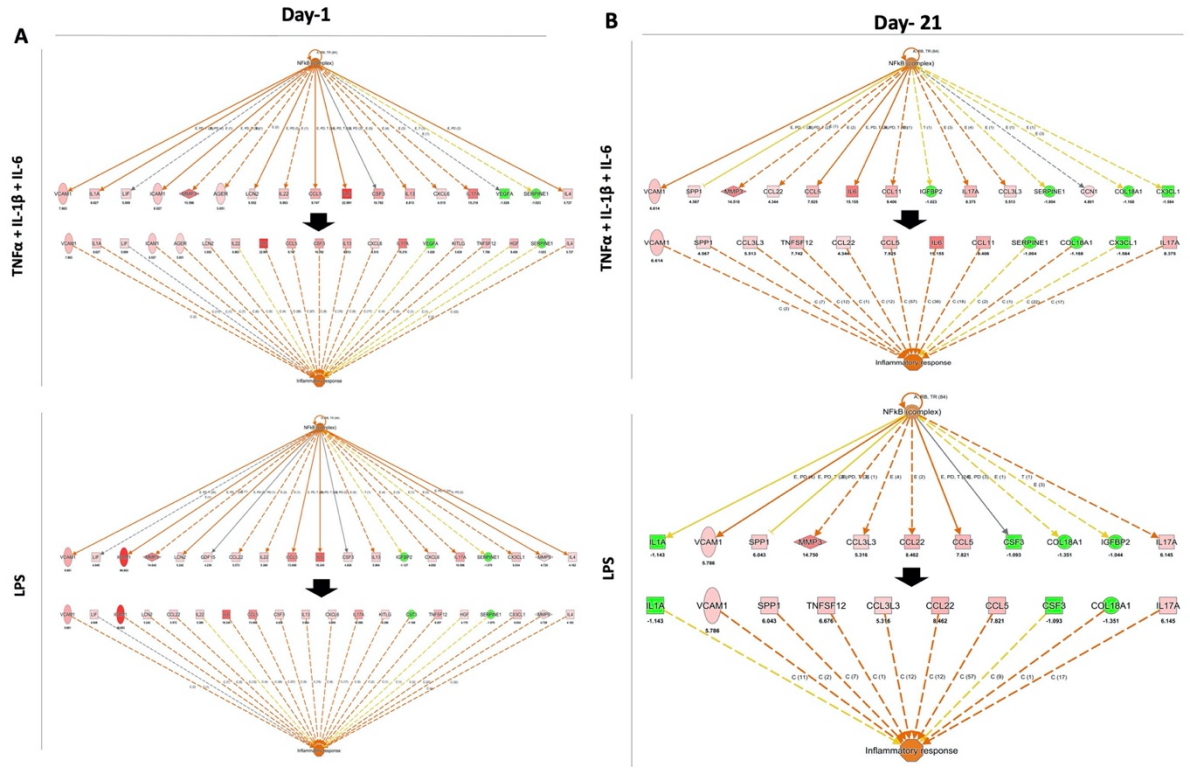

Figure S4: NFκB complex is directly or indirectly regulating the inflammatory response. Related to Figure 4.

Proteome profiler dataset was analyzed using IPA to demonstrate the prediction of upstream genes in NFκB complex and respective inflammatory response for each time point. The prediction shows a correlation between genes involved in NFκB pathway activation and inflammatory response upon cytokine combination (TNFα + IL-1β + IL-6) and LPS treatment at (A) day one and (B) day 21. The level of activation and type of genes involved were differentially regulated from day one to day 21 in both cytokine combination and LPS treatments. Also, between these two treatments, the level of activation and type of genes involved were unique. According to IPA, straight arrow: direct effect, dotted arrow: indirect effect and lines show predicted inhibition (green) or activation (orange) of the downstream genes.

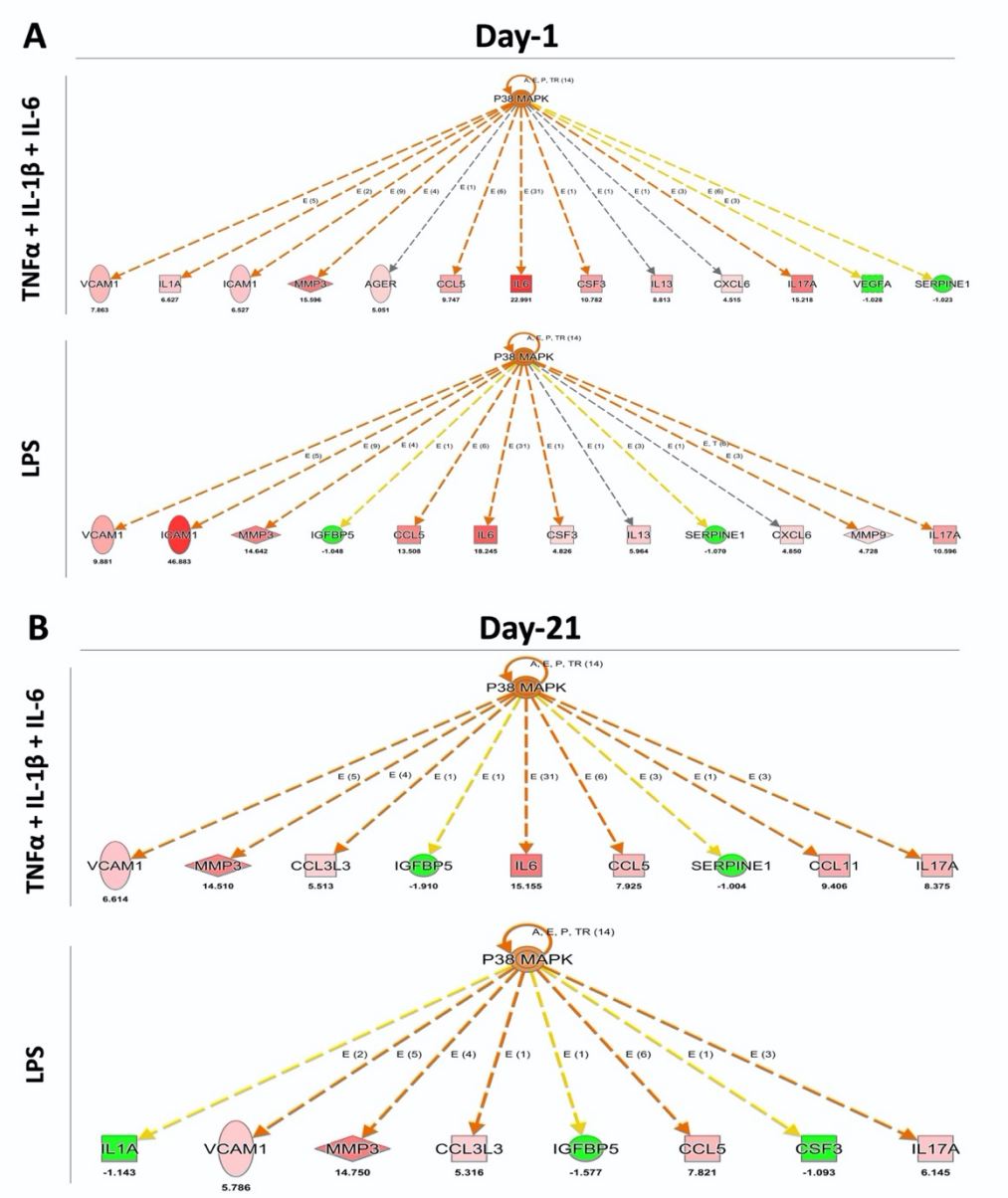

Figure S5: The p38-MAPK indirectly regulating genes involved in the inflammatory response. Related to Figure 4.

Proteome profiler dataset was analysed using IPA to demonstrate the prediction of upstream genes in the p38-MAPK pathway for each time point. The prediction shows a correlation between genes involved in the MAPK-p38 pathway leading to inflammation upon cytokine combination (TNFα + IL-1β + IL-6) and LPS treatment at (A) day one and (B) day 21. The level of activation and type of genes involved were differentially regulated from day one to day 21 in both cytokine combination and LPS treatments. Also, between these two treatments, the level of activation and type of genes involved were unique. According to IPA, dotted arrow: indirect effect and lines show predicted inhibition (green) or activation (orange) of the downstream genes.

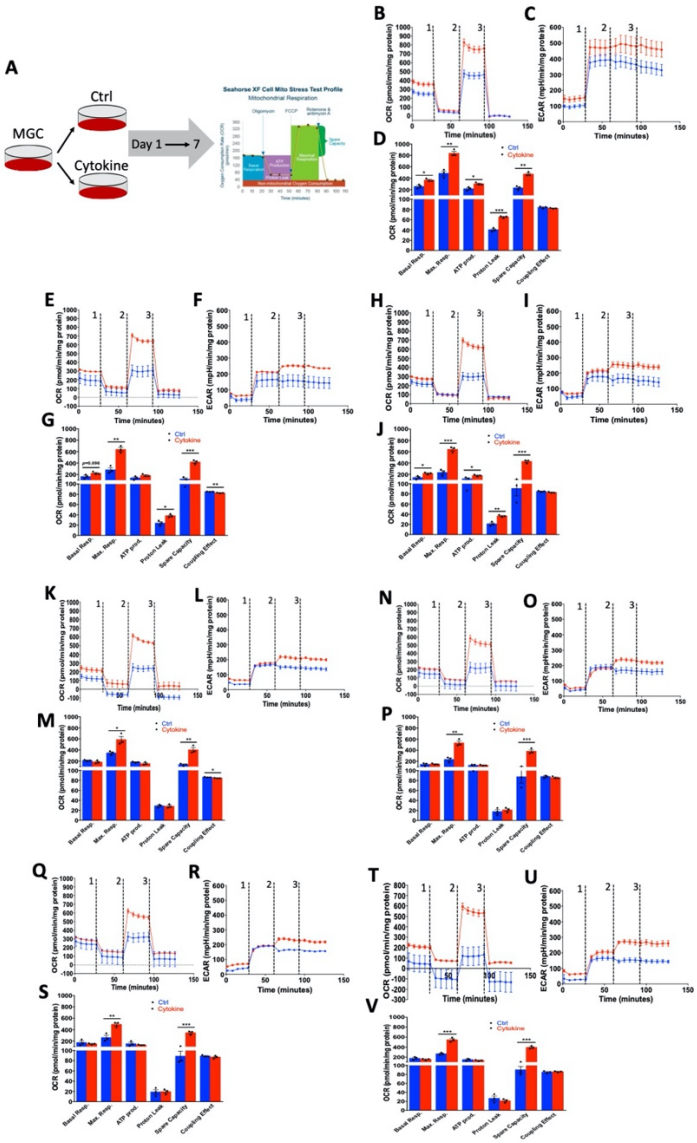

Figure S6: A cytokine combination treatment increases oxygen consumption rate (OCR), respiration, ATP production, proton leak and decreases coupling efficiency over seven days. Related to Figure 6. All parameters after performing seahorse XF cell mito stress test were calculated as a function of a cytokine combination treatment. For this, total protein per well was calculated using bicinchoninic acid (BCA) protein quantification assay and data was normalised against it. (A) Experimental plan. Day one (B-D), Day two (E-G), Day three (H-J), Day four (K-M), Day five (N-P), Day six (Q-S) and Day seven (T-V). (B, E, H, K, N, Q and T) OCR after the addition of three drugs (i.e. oligomycin, FCCP and Rotenone and antimycin A) sequentially. (C, F, I, L, O, R and U) Extracellular acidification rate (ECAR) after the addition of the above mentioned three drugs sequentially. (D, G, J, M, P, S and V) Six parameters: basal respiration, maximal respiration, ATP production, proton leak, spare capacity and coupling efficiency were measured and plotted as a bar graph. Data are represented as mean ± SEM, n= three experimental replicates. *p<0.05, **p<0.01, ***p<0.001 vs respective day of control. Unpaired t-test was performed to test the difference between the treatment and the respective day of control.

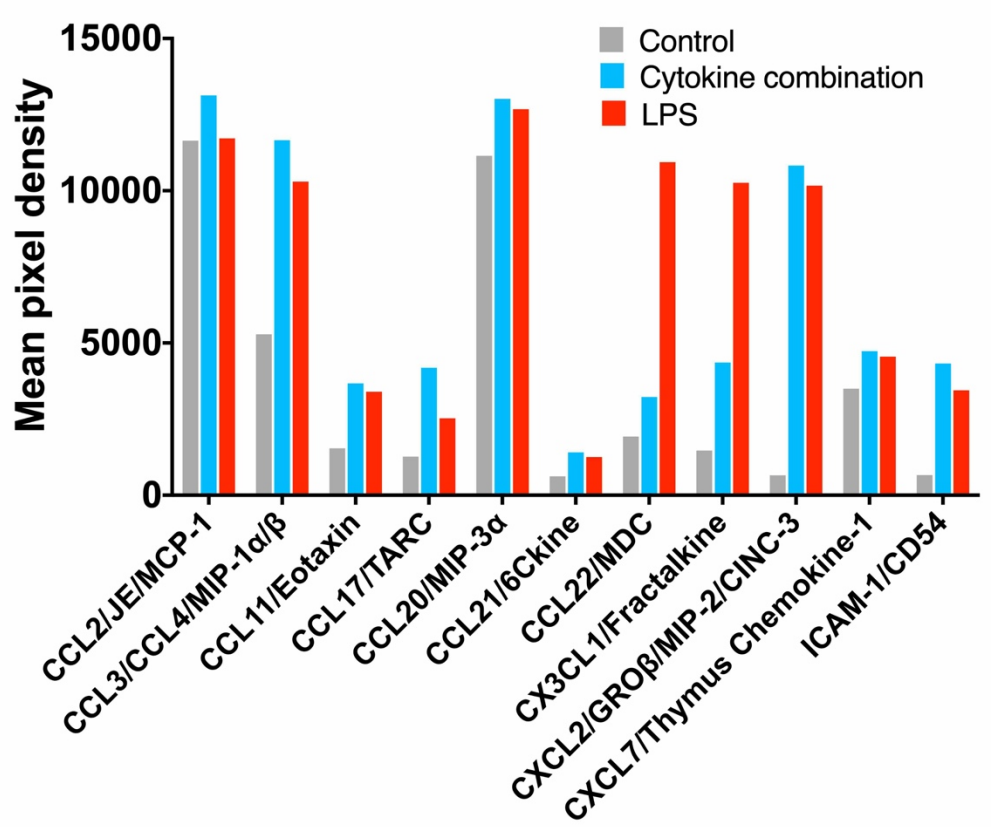

Figure S7: A panel of chemokines secreted by MGC after 24 hrs of treatment in the supernatant. Related to Figure 7.

The proteome profiler array data was analysed, and the mean pixel density plotted. A cytokine combination (i.e. TNF-α, IL-1β and IL-6 combination) was used along with LPS as a positive control. Each analyte was in duplicate. Based upon this data, cytokine-induced neutrophil chemoattractant (CINC)-3 (also called as CXCL2/ GROβ or MIP-2) was used for high-throughput screening (HTS) assay development.

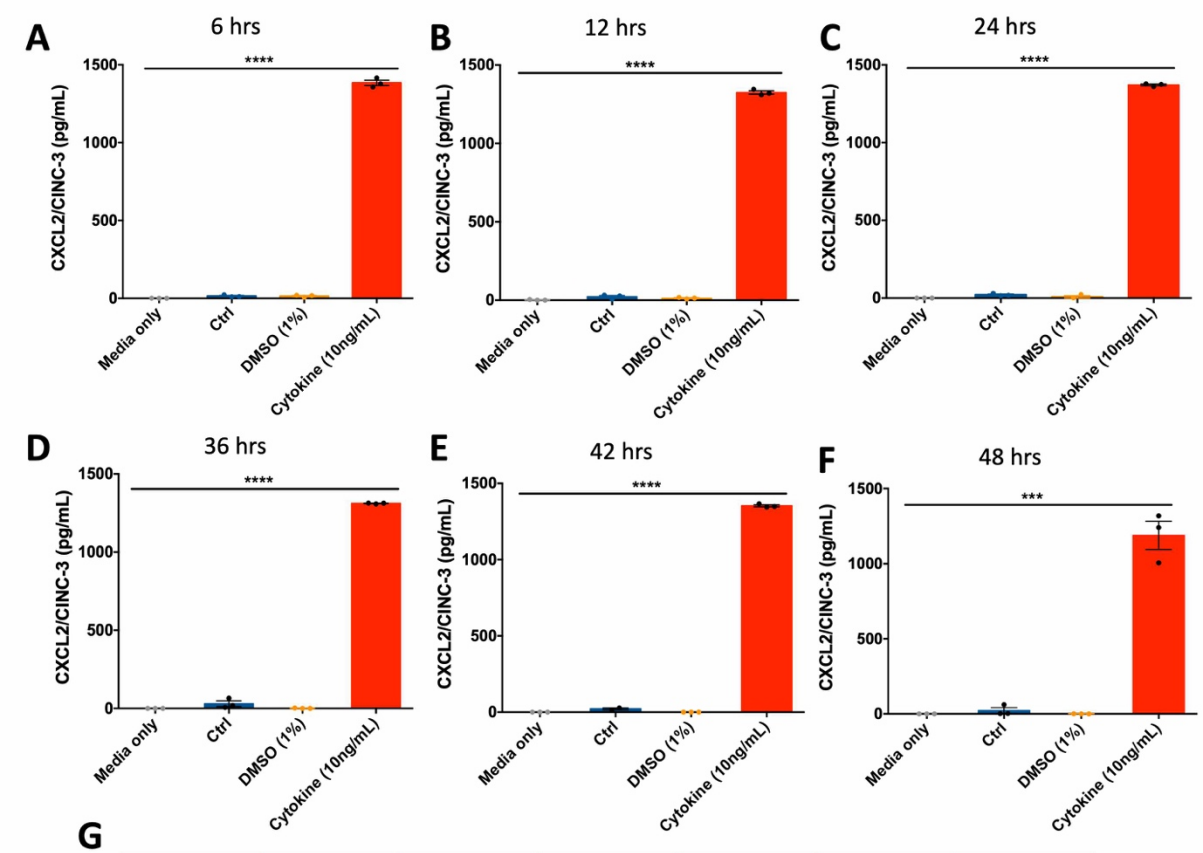

G

Hrs	6	12	24	36	42	48
Z' factor	0.92	0.93	0.96	0.92	0.95	0.49

Figure S8: CXCL2/CINC-3 expression after cytokine combination treatment. Related to Figure 7.

(A-F) CXCL2/CINC-3 production after the cytokine treatment after 6 (A), 12 (B), 24 (C), 36 (D), 42 (E) and 48 (F) hours. Data are represented as mean ± SEM, n= three experimental replicates, $^{****}p<0.0001$ and $^{***}p<0.001$; one-way ANOVA followed by *post hoc* Tukey test. (G) quality assessment of the assay: Z' factor after 24 hrs of cytokine treatment was higher than at other time points.

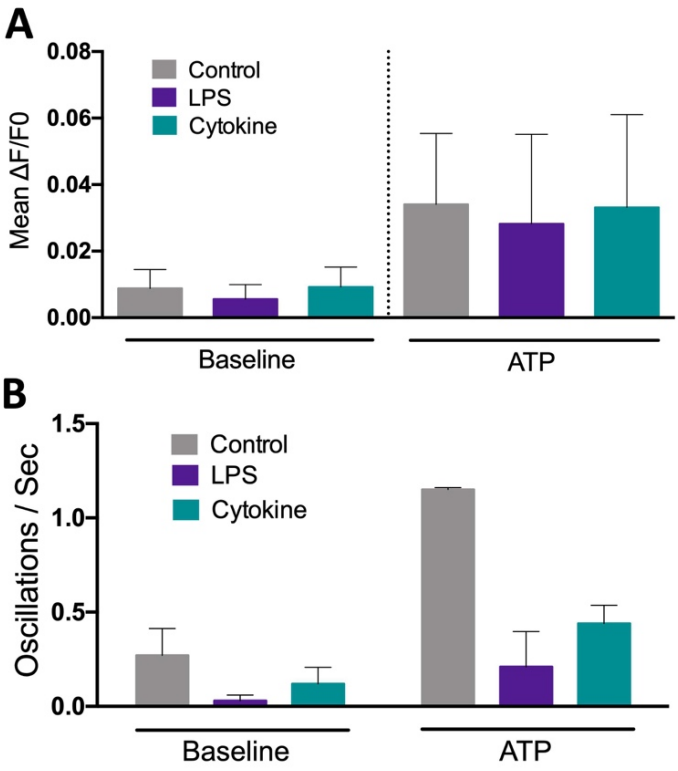

Figure S9: Effect cytokine combination and LPS on ATP induced endogenous intracellular Ca^{2+} signalling. Related to Figure 6.

MGC exhibited no effect of treatments on (A) amplitude (ΔF/F) of Ca2+ transient. However its (B) frequency was decreased upon both the treatments. Data is represented as mean ± SD, n= three technical replicates.

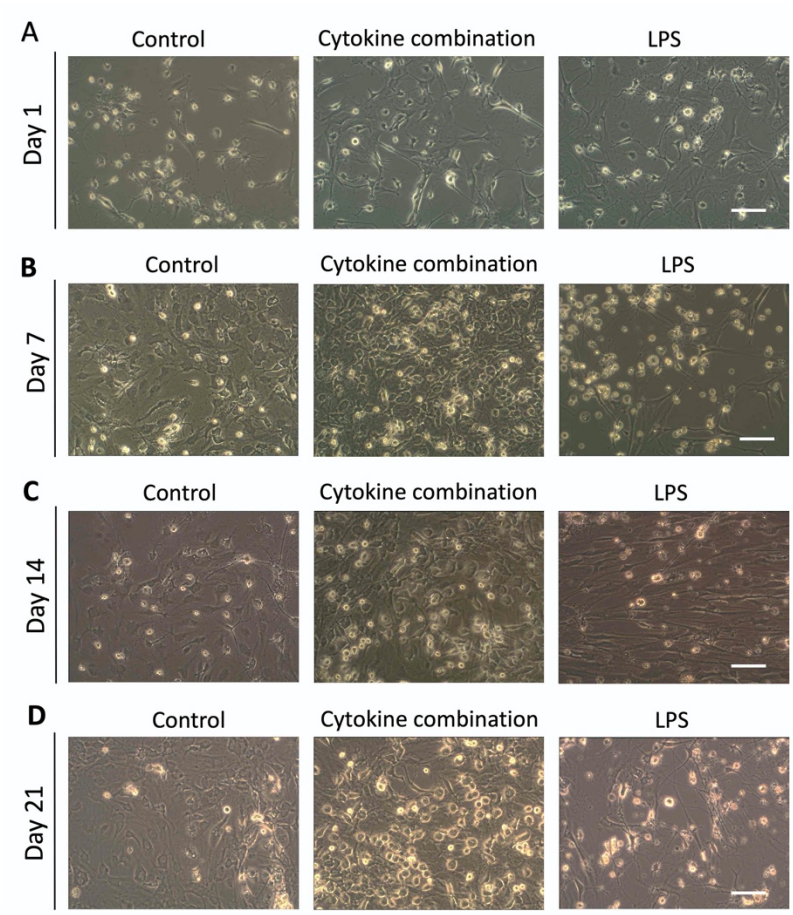

Figure S10: Phase contrast images of mixed glial cultures treated with cytokine combination and LPS at (A) day one, (B) day seven, (C) day fourteen and (D) day 21. Scale bar= 100 µm. Related to Figure 2.

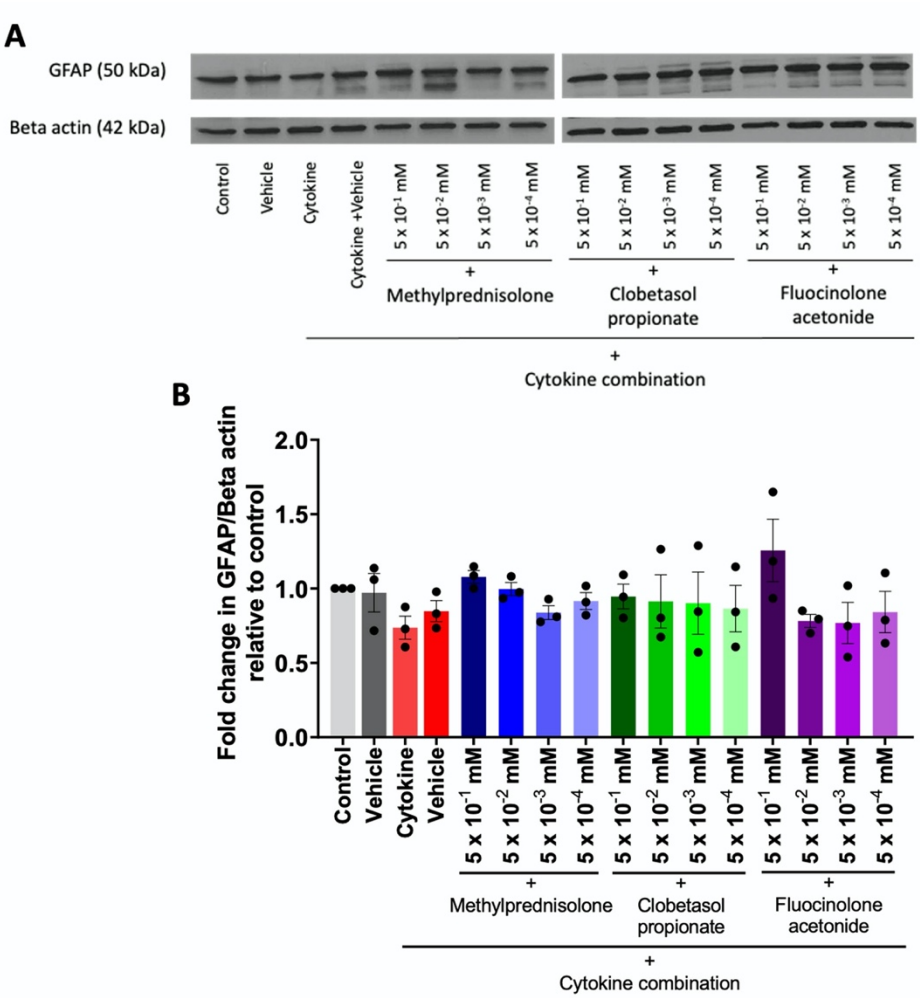

Figure S11: Validation of HTS- GFAP expression upon cytokine combination and corticosteroids treatment during secondary screening. Related to Figure 8.

(A) Western blots showing the expression of GFAP. We have selected three drugs from our primary screening, Methylprednisolone, Fluocinolone acetonide and Clobetasol propionate were treated with a concentration of 5 x 10-1 mM to 5 x 10-4 along with a cytokine combination treatment for 24 hrs. (B) Quantitative analysis of GFAP expression normalised with beta actin. Data are represented as mean ± SEM, n= three experimental replicates. One Way ANOVA. The fold change in GFAP expression was unchanged.

Table S2: Primary targets identified after high throughput screening. Related to Figure 7 and 8.

	(%) Alamar Blue reduced	CINC-3 (pg/mL)	Drug name	Function/ Use
1	96.52	551.53	Clobetasol Propionate	Corticosteroid, anti-inflammatory, antipruritic and vasoconstrictive
2	30.74	314.91	Idarubicin HCl	Cytotoxic anthracycline
3	110.30	534.04	Fluocinolone Acetonide	Anti-inflammatory and corticosteroid
4	105.62	699.12	Zidovudine (3'-Azido-3'-Deoxythymidine)	Thymidine analogue, reverse transcriptase inhibitor and inhibits protein glycosylation
5	104.18	790.36	Methylprednisolone	Anti-inflammatory and corticosteroid
6	7.67	160.32	Auranofin	Cytotoxic
7	110.26	-286.59	Goserelin Acetate	GnRH agonist
8	18.60	-2.03	Daunorubicin HCl	Cytotoxic anthracycline
09	42.14	428.22	Doxorubicin HCl	Cytotoxic anthracycline
10	103.48	792.78	Cefotaxime Acid	Semisynthetic cephalosporin antibiotic with bactericidal activity
11	117.78	456.27	Nystatin	Polyene antifungal drug
12	19.39	-81.41	Dactinomycin (= Actinomycin D)	Cytotoxic
13	32.59	356.48	Epirubicin HCl	Cytotoxic anthracycline

Transparent Methods

Cell culture

Primary MGCs were prepared from spinal cords as previously described (Kilcoyne et al., 2019). Spinal cords were isolated by the hydraulic extrusion technique from three-day-old postnatal rats, with minor modification in the spinal cord extrusion method (Kennedy et al., 2013). MGCs were cultured as previously described with slight modification in protocol (McCarthy and de Vellis, 1980). Briefly, meninges were gently peeled from spinal cords under a microdissection microscope. Spinal cords were chopped into fine (approx. 1 mm) pieces and digested using 1% trypsin-EDTA solution for 15-20 minutes. Trypsin activity was inhibited using DMEM-high glucose medium supplemented with 10 % fetal bovine serum (FBS) and 1% penicillin/streptomycin. Tissue was further digested by triturating it through various sizes of needles starting from 19G, 18G and then 23G. The digested tissue was expelled through a cell strainer filter (70 µM, Nitex Mesh, Falcon™), centrifuged and seeded into respective flasks. The MGCs were grown *in vitro* for three weeks before treatments were applied. Passage number one (P1) was maintained throughout all experiments.

Immunocytochemistry, microscopy and image analysis

MGC cells with a density of 1 X 10^5 cells/well were grown for two days on poly-L-lysine (PLL) coated coverslips in 24-well plates. On the day of staining, media was removed, and cells were washed with phosphate buffer saline (PBS). Fixed cells were permeabilized by incubating them in 0.2% Triton X-100 in PBS, followed by washing with PBS. Non-specific binding was blocked with 1% bovine serum albumin (BSA)+ 10% normal goat serum (NGS) in PBS solution (blocking buffer) for one hr at room temperature (RT). Primary antibody rabbit anti-GFAP (1:500, Dako, Z033429), mouse anti-CD11b (1:200 Sigma, CBL1512), mouse anti-Tubulin beta III isoform (1:200, Millipore, MAB1637) and rabbit anti-Olig2 (1:200, Millipore, AB9610) were prepared in blocking buffer and added to the plates, which were incubated overnight at 4^{o}C. After washing, cells were subsequently incubated with secondary antibody Alexa Fluor® 488 (1:500, Thermo Scientific™, A-10667) and Alexa Fluor® 546 (1:500, Thermo Scientific™, A11035) for one hr at RT. After washing, cells were then incubated in Hoechst 33342 (1:2000, Thermo Scientific™, 62249) for five min at RT. Coverslips were mounted onto glass slides using fluoromount and observed under the inverted fluorescent microscope.

Fluorescent cytochemistry images were captured on an Olympus VS120 Virtual Slide Microscope with Olympus VS fluorescence software (VS-ASW-FL). Every image for each time point was taken at the same exposure so that fluorescence intensity was consistent. Additionally, fluorescence intensity (FI) of lectin staining was quantitatively analysed using the ImageJ (Fiji) software. The number of Hoechst-

positive nuclei was quantified. Astrocytes cell morphology was assessed by two parameters, length and roundness of astrocyte processes, which were further, calculated by NeuronJ plugin and roundness measurement, respectively.

Flow cytometry:

For flow cytometry, mixed glial culture (MGC) cells were washed, trypsinised and suspended in flow cytometry staining (FACS) buffer. Cells were strained (Cell Trix®, 50 µm) and fixed with 2% paraformaldehyde (PFA) for 15 min at room temperature (RT) and washed with FACS buffer. Cells were permeabilised with 0.3% Triton in phosphate buffer saline (PBS) for 20 min at RT (not for the CD11b surface marker) and incubated in 3% BSA + 10% normal goat serum (NGS) for 30 min at RT. Cells were incubated with anti-glial fibrillary acidic protein (GFAP)- Alexa Fluor® 647 (1:20, BD Biosciences, 561470) and anti-CD11b/c-PE (1:20, ImmunoTools, 23159114) made in 1% BSA/PBS solution, for one hr at RT on ice. Cells were then washed with 1% bovine serum albumin/phosphate buffer saline (BSA/PBS), centrifuged, re-suspended in FACS buffer and acquired in the flow cytometer.

Optimisation of concentration of cytokines

MGCs were seeded at $5x10^5$ cells/well on poly-L-lysine (PLL) coated six-well plates or in 24-well plates. After growing in an incubator for two days, the media was replaced with no-serum media (Dulbecco's modified Eagle's medium (DMEM + 1% Penicillin/Streptomycin (P/S)). Cells were treated with four cytokine concentrations: 1, 10, 30 and 50 ng/mL, for 24 hrs.

Measurement of nitrite production

The nitrite concentration was assessed by the colorimetric reaction of the Griess reagent (Molecular Probes, Inc., G-7921). Briefly, after treatments on MGC for specific time points, the supernatant was collected from each group, and an assay was performed according to the manufacture's protocol. Griess reagent prepared nitrite concentration was calculated from a standard curve using sodium nitrite.

Study design for chronic inflammation (21 days) of MGC

MGCs were seeded at $5x10^5$ cells/well on PLL-coated six-well plates or in 24-well plates. After growing in an incubator for two days, media was replaced with low-serum media (DMEM + 1% P/S + 1% FBS) and cells were treated with 10ng/mL of three cytokines (TNF-α, IL-1β, and IL-6) (R & D Systems; recombinant rat TNF-alpha protein, 510-RT-010; recombinant rat IL-1 beta/ IL-1F2 protein, 501-RL-010; recombinant rat IL-6 protein, 506-RL-010) at day zero and every subsequent two days (i.e. day 0,

2, 4, 6, 8, 10, 12, 14, 16, 18 and 20) until day 21. Multiple combinations of these three cytokines were used as listed in Table S1. At each of the treatment time points (except day zero), half of the media was changed and filled with new cytokine treatment media. 100ng/mL dose of LPS (Sigma-Aldrich) was given in the same procedure as a positive control. Finally, a negative control was carried out by performing the same half-media change procedure with low-serum media. All experiments were run with three biological replicates. The supernatant was collected, and protein was isolated at respective time points for further analysis.

Western blotting

MGC cells of density 5 x 10^5 cells/mL were seeded into six-well plates and after respective treatments, cells were lysed in a radioimmunoprecipitation assay (RIPA) buffer (50 mM Tris-HCl, pH 8.0, 150 mM NaCl, 0.02% sodium azide, 0.1% sodium dodecyl sulphate (SDS), 1% Nonidet P-40, 0.5% sodium deoxycholate) (Sigma-Aldrich, R0278) with a protease inhibitor cocktail (1:100) (cOmplete™, EDTA-free, Roche, Inc., 11873580001), phenylmethylsulfonylfluoride (1:50) (Sigma-Aldrich, 93482) and phosphatase inhibitor cocktail (1:10) (PhosSTOP™, Roche, Inc., 04906845001). The protein concentration in the total cell lysate was determined using a bicinchoninic acid (BCA) protein assay kit (Pierce™ BCA Protein Assay Kit, Thermo Fischer Scientific, 23225). An equal amount of protein from each sample was separated by 10-12% SDS polyacrylamide gel electrophoresis and transferred to Hybond® ECL™ nitrocellulose membrane. Membranes were stained with Ponceau S to visualize successful transfer and protein loading. The membrane was blocked with either 5% milk or 5% BSA depending upon the suitability of primary antibodies to avoid non-specific binding of antibodies. This was followed by primary antibody incubation overnight at 4^{o}C with 1:2000 rabbit anti-P-NFκB-p65 (Ser536) (93H1) (Cell Signalling, 3033s), 1:200 mouse anti-NFκB-p65(F-6) (Santacruz Biotech, sc-8008), 1:1000 P-p38 MAPK (Thr180/Tyr182) (Cell Signalling, 3033s), 1:200 mouse anti-p38α/β MAPK (Santacruz Biotech, sc-7972), 1:1000 mouse anti-GFAP (Sigma, G3893), 1:2000 rabbit iNOS (Thermo Fisher Scientific, PA3-030A) or one hour at RT with 1:15,000 anti-β-actin (Sigma, A5441) on a rocking platform. All washing steps were carried out in Tween-20 in TBS (0.1%). Next, horseradish peroxidase-conjugated secondary goat anti- rabbit or goat anti-mouse antibodies (prepared in 5% milk or 5% BSA at 1:10,000) were applied, followed by enhanced chemiluminescence detection. Signals from protein bands were captured on x-ray films (CL-XPosure™ Film, Thermo Scientific™, 34090), which were further analysed using Image Studio™ Lite software and signals recorded as pixel density.

Proteome profile array

The Rat XL Cytokine Proteome Profiler™ Array kit (ARY030, R&D SYSTEMS) was used to assess the parallel determination of relative expression of chemokines, pro- and anti-inflammatory cytokines and growth factors secreted by MGCs. The assay was carried out as per the manufacturer's procedure given for the supernatant. Positive signals could be seen on X-ray films (CL-XPosure™ Film, Thermo Scientific™, 34090) which were further analysed using Image Studio™ Lite software and signals recorded as pixel density. Further 'mean pixel density' from each analyte was calculated, and the data plotted as a heatmap. Hierarchical clustering of the data was performed using Morpheus, https://software.broadinstitute.org/morpheus.

Ingenuity pathway analysis (IPA)

The proteome profiler™ data were normalised with the control (untreated) group and uploaded into IPA software© (QIAGEN). Based upon distribution analysis of the data, a cut-off of 1.5 for downstream molecules and upstream molecules was set. A comparative analysis was carried out to understand the effect of molecules on biological functions and diseases. Further regulator network analysis and canonical pathway analysis were performed.

Cellular stress assay

40,000 MGC cells/well were seeded into the XFp Seahorse miniplates. After growing in an incubator for two days, the cytokine treatment was given only for seven days as described above in the "Study design for chronic inflammation of MGC" section. On the day of assay, the media was replaced with glucose, pyruvate, L-glutamine and phenol red-free Seahorse XF base medium. Assay medium was prepared with the addition of glucose (25 mM), sodium pyruvate (1.0 mM) and L-glutamine (2.0 mM). The pH was adjusted to 7.4 using 1N NaOH, and the media was filtered through a 0.2 mm filter. Before the assay, the sensor cartridge was hydrated overnight, and Seahorse instrument was turned on at least five hrs before the assay. Oxygen consumption rate (OCR) and extracellular acidification rate (ECAR) was measured on an XFp Seahorse analyser with the sequential addition of one. Oligomycin (1 uM), 2. FCCP (2 uM), 3. Rotenone/antimycin (0.5 uM) for 110 minutes with five readings per cycle.

After the assay was completed, cells were lysed in RIPA buffer, and the protein concentration was determined using a BCA protein assay kit (Pierce™ BCA Protein Assay Kit, Thermo Scientific™, 23225). OCR and ECAR data were normalised on Wave Controller software using protein concentration per well. The extracellular acidification and rate of adenosine triphosphate (ATP) production by glycolysis and oxidation were calculated using ECAR and OCR values (Mookerjee et al., 2015).

In vitro reactive oxygen species *(*ROS)/superoxide detection

20,000 MGC cells/well were seeded into the specialised PLL coated 384-well plates (Greiner Bio-one CELLCOAT®). After growing for two days, the media was replaced with FBS-free media (DMEM +1% P/S). Cells were treated with a combination of pro-inflammatory cytokines (tumour necrosis factor-α (TNF-α), interleukin (IL)-1β and interleukin (IL)-6) of dose 10 ng/mL for 24 hrs. After the treatment, media was removed, and the protocol was followed as given in ROS-ID® total ROS/superoxide detection kit, ENZ-51010. Fluorescence was measured at Ex/Em: 490/525 nm to detect ROS in cells and data was presented as a bar graph.

Calcium imaging

Calcium imaging was performed as previously described with some modifications (Avazzadeh et al., 2019). After 24 hr of treatments, MGCs were washed with warm Krebs-Ringer's buffer, incubated with 1μM Fluo-4 AM (ThermoFisher scientific, F14201) in Krebs-Ringer's buffer for 40 min at 37°C in the incubator. Cells were further washed and left with fresh Krebs-Ringer's buffer for 20 min in the incubator. Images were taken in an imaging chamber (Warner Instruments, Inc., RC-26GLP) on a Zeiss Axiovert 200 microscope (× 10) for total 180 sec, 60 sec with baseline and 120 sec with adenosine triphosphate (ATP) (10 μM) as an inducer. Videos were captured with a Hama-matsu ORCA284 at 1 Hz frame rate. FluoroSNNAP in MATLAB (MathWorks, Inc.) was used to analyse images. A fluorescence ratio ($\Delta F/F_0$) and oscillations per sec were calculated.

Screening assay development (optimisation and validation of ELISA assay to detect CINC-3)

15,000 MGC cells/well were seeded into the specialized PLL-coated 384 well plates (Greiner Bio-one CELLCOAT®). After growing for two days, the media was replaced with 50 μL of FBS-free media (DMEM +1% P/S) and cells were treated with a combination of pro-inflammatory cytokines (TNF-α, IL-1β, and IL-6) of dose 10 ng/mL (per cytokine) for 6, 12, 24, 36, 42 and 48 hr. After the treatment, 30 μL of media was collected, and ELISA (CINC-3) (DuoSet®, Rat CXCL2/CINC-3 ELISA, DY525, R&D Systems) was performed using high binding affinity 384-well clear plates (Nunc® MaxiSorp™ 384-well plates, Sigma, P6366). Assay Z' factor was calculated to evaluate the suitability of this assay (Zhang et al., 1999).

$$\mathrm{Z'Factor} = 1 - \frac{3(\sigma_\rho + \sigma_n)}{|\mu_\rho - \mu_n|}$$

This assay was performed using JANUS® automated liquid handling workstation (Perkin Elmer) and Thermo Multidrop 384 Dispenser (Thermo Fischer Scientific). 15,000 cells/well were seeded into the specialized PLL-coated 384 well plates. After the treatment, 30 μL media was transferred to high

binding affinity 384-well clear plates using a JANUS® workstation to perform ELISA (CINC-3). Later steps were carried out using a Thermo Multidrop 384 Dispenser. Further, the Z' factor was calculated to evaluate the suitability of this assay under automated conditions.

High-throughput drug screening to identify hits with anti-inflammatory properties

15,000 MGC cells/well were seeded into the specialized PLL-coated 384 well plates (Greiner Bio-one CELLCOAT® using JANUS® automated workstation, and the treatment was given after two days. On the day of treatment, the drug compounds (10 mM) were resuspended in 60 µL of FBS-free media (DMEM +1% P/S) with the combination of pro-inflammatory cytokines (TNF-α, IL-1β, and IL-6) of dose 10 ng/mL (per cytokine). Drugs were incubated for one hr at RT. Further, media from the cell containing PLL-coated plates was removed, and 50 µL of media/treatment containing drug compounds was transferred to cell plates. The final concentration of compounds was 3 µM and 0.03% DMSO v/v in each assay well. After 24 hr of treatment, 30 µL of supernatant from each assay well was transferred to high binding affinity 384-well clear plates to perform ELISA for CINC-3). Later steps were carried out using Thermo Multidrop 384 Dispenser. The optical density (450 and 540 nm) of each well was determined immediately, reading at 540 nm was subtracted from the reading at 450 nm. To analyse the effect of drugs on inflammation, a cut-off of 50% reduction in the CINC-3 expression was applied. Further to assess cell viability, 20 µL of 10% solution of alamarBlue™ was added per well containing 20 µL of previous treatment media. Fluorescence was measured at Ex 531/Em 595 after five hours of incubation in the incubator at 37°C. All samples were normalised to DMSO (0.03%) control group.

The secondary screening was performed using selected hit compounds such as methylprednisolone (LKT-M1877-M100, Enzo Life Sciences), fluocinolone acetonide (LKT-F4582-M025, Enzo Life Sciences) and clobetasol propionate (LKT-C4659-M100, Enzo Life Sciences) to validate the primary screening. 20,000 MGC cells/well were seeded into the specialized PLL-coated 96-well plates. After growing for two days, the media was replaced with 100 µL of FBS-free media (DMEM +1% P/S) and cells were treated with a combination of pro-inflammatory cytokines (TNF-α, IL-1β, and IL-6) at 10 ng/mL (per cytokine) for 24 hr. 30 µL of supernatant from each assay well was transferred in high binding affinity 384-well clear plates, and ELISA (CINC-3) was performed as per the manufacturer's protocol. Later alamarBlue™ assay (Bio-Rad) was performed on cells as per manufacturers protocol.

Statistical analysis

All statistical analyses were done using GraphPad Prism 8.00 software, Inc. Most data were analysed by one-way analysis of variance (ANOVA) followed by Tukey multiple comparison test for comparing more than three samples, and two-tailed unpaired *t*-tests for comparing two samples with 95% confidence. Non-parametric data were analysed by the Mann-Whitney U test for comparing two samples with 95% confidence. $p < 0.05$ was considered to be statistically significant.

Supplemental References:

Avazzadeh, S., McDonagh, K., Reilly, J., Wang, Y., Boomkamp, S. D., McInerney, V., Krawczyk, J., Fitzgerald, J., Feerick, N. & O'Sullivan, M. (2019). Increased ca 2+ signaling in nrxn1α+/− neurons derived from asd induced pluripotent stem cells. *Mol. Auti.,* 10**,** 1-16.

Kennedy, H. S., Jones, C., 3rd & Caplazi, P. (2013). Comparison of standard laminectomy with an optimized ejection method for the removal of spinal cords from rats and mice. *J. Histotech.,* 36**,** 86-91.

Kilcoyne, M., Patil, V., O'Grady, C., Bradley, C. & McMahon, S. S. (2019). Differential glycosylation expression in injured rat spinal cord treated with immunosuppressive drug cyclosporin-a. *ACS Omega,* 4**,** 3083-3097.

McCarthy, K. D. & de Vellis, J. (1980). Preparation of separate astroglial and oligodendroglial cell cultures from rat cerebral tissue. *J. Cell. Biol.,* 85**,** 890-902.

Mookerjee, S. A., Goncalves, R. L. S., Gerencser, A. A., Nicholls, D. G. & Brand, M. D. (2015). The contributions of respiration and glycolysis to extracellular acid production. *Biochim. Biophys. Acta.,* 1847**,** 171-181.

Zhang, J. H., Chung, T. D. & Oldenburg, K. R. (1999). A simple statistical parameter for use in evaluation and validation of high throughput screening assays. *J. Biomol. Screen.,* 4**,** 67-73.